Chapter 3
Design, Synthesis and Application of Metal Oxide-Based Sensing Elements: A Chemical Principles Approach

Valery Krivetskiy, Marina Rumyantseva and Alexander Gaskov

Abstract The chemical approaches to improvement of selectivity of semiconductor metal oxide gas sensors are the main subject of this chapter. Current concepts of interrelationships between metal oxide chemical composition, crystal and surface structure and its activity in the reaction with gas phase components are considered. Application of such concepts to the design of sensor materials based on nanocrystalline SnO_2 is discussed thoroughly. Experimental data concerning chemical composition, solid–gas chemical interaction activity and sensor properties is given and critically analysed. The possibility of utilization of solid–gas chemical reaction activity concepts for directed synthesis of new metal oxide semiconductor sensor materials with selective response to given gases is highlighted.

3.1 Introduction

A major shortcoming of SnO_2 as a material for gas sensors is its low selectivity, due to the presence of a wide range of adsorption sites on its surface that cannot distinguish the contribution of each type of molecule in the gas phase to the total electrical signal. One of the ways to improve its selectivity is the surface modification of a highly dispersed oxide matrix with clusters of transition metals or their oxides, which may affect the electrophysical and chemical properties of the surface. Quite a number of approaches has been suggested to date to direct the choice of modifiers for sensor materials, using the values of electronegativity [1], changes in work function [2], as well as structural properties of oxides of d-elements [3] as correlation parameters.

For sensors targeting sulfur-containing gases (in particular hydrogen sulfide) it was proposed [1] to select a modifier based on the electronegativity values of the

V. Krivetskiy · M. Rumyantseva · A. Gaskov (✉)
Lomonosov Moscow State University, Moscow, Russia
e-mail: gaskov@inorg.chem.msu.ru

M. A. Carpenter et al. (eds.), *Metal Oxide Nanomaterials for Chemical Sensors*, Integrated Analytical Systems, DOI: 10.1007/978-1-4614-5395-6_3,

corresponding cations. It was assumed that the bond formation between the sulfur ion and metal cation with low electronegativity leads to a weakening of the S–H bond and facilitates the dissociation of the molecule. Another approach is based on the change in work function during the chemisorption of molecules from the gas phase on metal surfaces [2]. The magnitude of this change depends on the nature of the metal and the gas molecules, and likely enables the selective detection of gases using planar structures of a metal/semiconductor interface, as well as with polycrystalline systems in which metal clusters are distributed on the surface of the semiconductor.

Certain predictions on sensitivity and selectivity of sensor materials can be made based on the catalytic activity of transition metals and their oxides. Possible mechanisms for the catalytic effect of additives on the sensor properties of the material were proposed [4]:

- the effect on the rate of Redox reaction, which leads to higher sensitivity and better dynamic properties at low operating temperatures;
- formation of intermediates, which can change the conductivity of SnO_2;
- the impact on the surface coverage and rate of adsorption.

Different concepts of heterogeneous catalysis allow linking the physical, chemical and electronic properties of materials and their catalytic activity in different processes [5]:

- acid–base catalysis theory, based on the number and strength of acidic and basic centers on the catalyst surface;
- the theory of "structural matching" assumes that an active center—an ensemble of atoms having some specific size and structure—is needed for the reaction on the surface to take place;
- the electronic theory of catalysis on semiconductors [6], the concept, based on the correlation of catalytic activity and electronic structure of the material, which includes consideration of the quantum-size effects with decreasing particle size to the nanometer range.

However, there is scarce number of works that use the reasoned choice of modifiers for sensor materials surfaces. In the development of SnO_2-based gas sensors the representatives of all families of chemical elements: noble metals and oxides of s-, p-, d- and f-elements, have already been tested as modifiers (Fig. 3.1). In most cases, the results are obtained by "trial and error" effort and do not imply correlations between the properties of the modifier and sensor performances to the target gas.

3.2 Reactivity of Oxide's Surface in Solid-Gas Interaction

This section discusses the approaches described in the literature to assess the acid–base and Redox surface properties of metal oxides, based on their chemical composition, oxidation state of the metal, coordination environment and crystal structure.

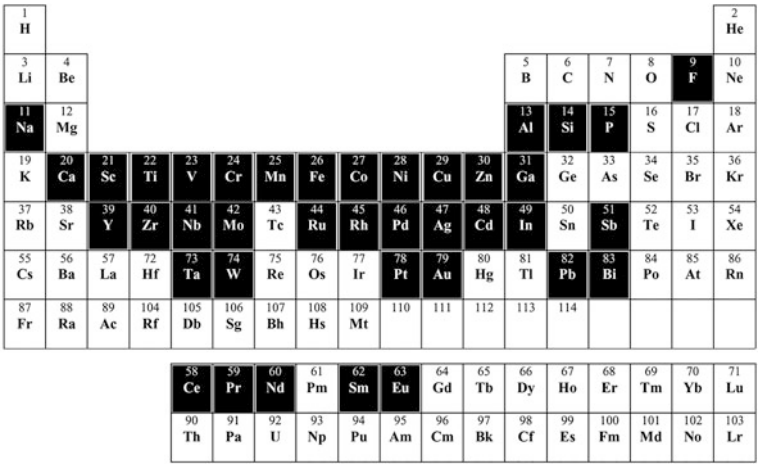

Fig. 3.1 Elements that have been tested as modifiers in the development of SnO_2 based gas sensors

3.2.1 Adsorption–Desorption Interactions, Acid–Base Properties

The key chemical process that leads to the emergence of a sensor response in the presence of any detectable component is the adsorption (chemisorption) of gas molecules on the surface. This process is usually considered in terms of a Lewis acid–base interaction [7]. The active sites of adsorption on a metal oxide surface are coordinatively unsaturated metal cations and oxygen anions. Metal cations as electron-deficient atoms having vacant orbitals, exhibit Lewis acid properties, while oxygen anions act as bases.

The main problems in the synthesis of new materials with a well defined surface acidity are (1) a quantitative description of the changes in acidity made by modification and especially (2) predicting the reactivity of the newly created composites. The advances in IR-spectroscopic methods of probing molecules [8, 9], their thermo-programmed desorption [10] and microcalorimetric methods [11], allow a quantitative comparison of the acidity of the synthesized materials. It is important to emphasize that the acidity of the metal cation in the oxide surface is defined by a set of parameters: the type and oxidation state of the cation, the presence of defects on the surface, and the number of vacancies in the anion sublattice, which is different in the oxidized and reduced state of the surface [7]. At the same time, the acidity and reactivity of the metal oxide surface are closely associated with the "bulk" properties of the phases present [5].

In the 1970s Duffy proposed a universal approach which, allows ranking of various metal oxides on their Lewis acidity and introduced a new notion of the so called optical basicity of oxides [12]. This value characterizes the degree of "red" shift (towards longer wavelengths) of characteristic bands in UV absorption

spectra corresponding to the $^1S_0 \rightarrow {}^3P_1$ transitions of probe ions (Tl^+, Pb^{2+} or Bi^{3+}), embedded in an oxide structure. This shift is caused by the expansion of the outer electron orbitals of the cations (acidic centers), surrounded by anions (basic centers). This so called nephelauxetic effect is based on the covalent interaction between the central cation and its surrounding ligands, which leads to the formation of molecular orbitals with a predominant contribution of orbitals from the central cation. The expansion is due to the fact that the formed boundary molecular orbitals are antibonding in nature, and also due to increased screening of the positively charged nucleus of the cation. On the example of complex-forming metal cations, this effect is manifested as a change in the absorption spectra corresponding to the energy transitions of d-electrons. Orbital expansion is accompanied by the weakening of electron repulsion forces and, consequently, the partial degeneracy of the energy sublevels of the excited states surrounded by the ligands (Lewis bases), one can estimate the degree of this acid–base interaction. According to this concept, the bulk Lewis acidity of the cations forming the oxide can be estimated to be inversely proportional to the basicity of oxygen anions. It can be determined by measuring the magnitude of the nephelauxetic effect arising in its absorption spectrum with introducing a probe d-element cation into the oxide matrix. The more the red shift of spectral bands caused by the expansion of the outer orbitals of the cation, the more the basicity of oxide and the weaker the Lewis acidity of its constituent cations.

By generalizing the experimental data obtained in the course of studying the optical basicity of silicate oxide glasses of different compositions, it has been shown [13] that the optical basicity Λ is an additive quantity, and therefore, the majority of individual oxides can be classified based on measured values of optical basicity of glasses of known composition:

$$\Lambda_{th} = X_{AO_{a/2}}\Lambda(AO_{a/2}) + X_{BO_{b/2}}\Lambda(BO_{b/2}) + \ldots, \tag{3.1}$$

$\Lambda(AO_{a/2})$, $\Lambda(BO_{b/2})\ldots$ optical basicity of oxides $AO_{a/2}$, $BO_{b/2}$ …
$X_{AO_{a/2}}$, $X_{BO_{b/2}}\ldots$ proportion of oxygen atoms, provided by each oxide

Optical basicity of simple oxides, of the substance, is correlated with other fundamental parameters. It has been shown [14] that Λ is proportional to the electronegativity of the metal, which is forming the oxide:

$$\Lambda = 0.75/(\chi_M - 0.25) \tag{3.2}$$

χ_M Pauling electronegativity of metal cation

Another type of correlation is related to the so-called polarizability of the oxygen atom in the oxide, α_O^{2-} [13]:

$$\Lambda = 1.67\left(1 - 1/\alpha_O^{2-}\right) \tag{3.3}$$

The polarizability of the oxygen atom, reflecting the tendency of electrons involved in chemical bonding to move from of the ionic core in the presence of an external electric field, is calculated from the molar polarizability of simple oxides:

$$\alpha_m\left(A_iB_j\right) = i\alpha_A + j\alpha_B, \tag{3.4}$$

A :cation
B :anion
i and j :their stoichiometric coefficients in oxide

Molar polarizability of oxide can be calculated from the refractive index of the oxide according to the formula of Lorentz-Lorenz (also known as Clausius-Mozotti equation) [13, 15]:

$$\alpha_m = \frac{3V_m}{4\pi N}\frac{n^2-1}{n^2+2} \tag{3.5}$$

V_m -molar volume
N -Avogadro number
n r-efractive index

Thus, it is possible to estimate the strength of acid centers on the surface of an oxide material using the bulk properties of the compound and the fundamental parameters of its constituent atoms. This simple approach has its drawbacks. The more important one is that the calculations are based on Pauling electronegativity values of the cations with no regard of the structural features of oxides and, consequently, neglects their effect on the electronegativity. As a result this approach was suitable only for compounds with ionic metal—oxygen bonds.

In 1982 Zhang for the first time made an attempt to create a quantitative Lewis acidity scale of various cations [16]. He found the approach to the quantitative description of the ion contribution to the metal—oxygen bond through the so-called polarizing power of the cation. The polarizing power P can be calculated as:

$$P = Z/r_k^2 \tag{3.6}$$

Z formal cation charge
r_k ionic radius

At the same time Zhang has developed a scale of electronegativities of the elements [17], calculated from the thermodynamic parameters using the formula:

$$\chi_Z = \frac{0.24n^*(I_z/R)^{1/2}}{r^2} + 0.775 \tag{3.7}$$

r covalent metal radius
I_z ionization potential

R Rydberg constant
n^* effective main quantum number

Covalent components of the metal–oxygen bond in the metal oxide compounds, according to Zhang, are determined by their electronegativity. The value of Lewis acidity Z is determined by the formula:

$$Z = P - 7.7\chi_Z + 8.0 \tag{3.8}$$

Zhang was able to rank a large number of cations. However, this scale is not valid for small cations with high nuclear charge. Portier et al. [18] proposed a new parameter related to acid strength, taking into account the ionic-covalent character of the metal–oxygen bond in oxides (ionic-covalent parameter, ICP):

$$ICP = \log P_i - A\chi_i + B \tag{3.9}$$

P_i polarizing power
χ_i electronegativity

The coefficients A and B are chosen, so that the ICP of Au^+ cation was zero [19]. This cation acts as a reference due to its extremely low acidity and instability of compounds, even with very strong bases. Using this parameter authors have been able to carry out a quantitative classification of Lewis acidity of about 500 cations in different oxidation states and coordination environments.

Further attempts were made to develop the concept of optical basicity on the basis of a quantitative understanding of the ionic-covalent character of metal–oxygen bond in oxides. These approaches are based on the linear correlation of the optical basicity of alkali and alkaline earth metal oxides with ICP. Using the method of linear regression five different linear correlations between the optical basicity and the ionic-covalent parameter of different types of cations (s-p, $d^{10}s^2$, d^0, d^1–d^9, d^{10}) were subsequently established [20]. The quantitative relationship between the Lewis acidity and the fundamental parameters of the substance identified in this way can be used to predict the reactivity of not only the individual oxides, but also composite materials based on them Fig. 3.2.

Another approach that is widely used in predicting the reactivity of oxide materials, is the principle of electronegativity equalization developed by Sanderson, and the corresponding scale of electronegativities of the elements [21, 22]. Sanderson started from the principle that the formation of the ionic part in the chemical bonding between atoms of different nature is inevitably accompanied by a decrease in its covalent component. This is due to the redistribution of electron density between the atoms that form a chemical compound. This redistribution, in turn, induces a charge which balances the difference in the electronegativity of atoms. Thus, the compound acquires certain electronegativity, which is the geometric mean of electronegativities of its constituent atoms.

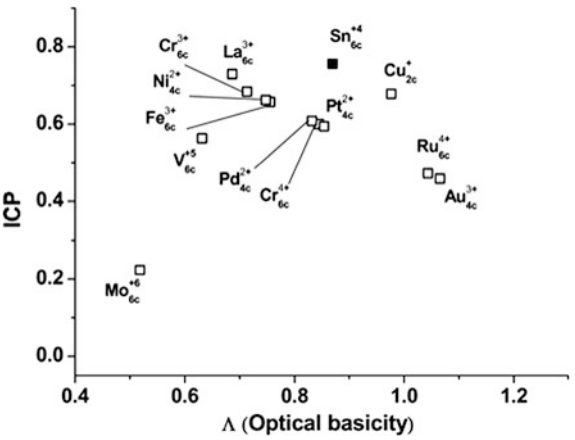

Fig. 3.2 The scale of optical basicity of selected cations based on their oxidation state, coordination number and electronegativity [20]

Sanderson's concept allows us to calculate the partial charges on the atoms forming the compound, reflecting the contribution of the ionic component of a chemical bond directly from the values of the electronegativities of the cations.

$$\sigma_M = 0.48 \times \left(\sqrt[x+y]{(S_{M^+})^x (S_{Ch})^y} - S_{M^+} \right) \times S_{M^+}^{-1/2} \tag{3.10}$$

σ_M cation partial charge
S_{M^+} cation electronegativity
S_{Ch^-} chalcogen electronegativity (for oxygen S = 3.61)
x, y stoichiometric coefficients

To date, these values are known for a large number of cations in various formal oxidation states, so one can easily rank the corresponding oxides by their Lewis acidity (Fig. 3.3). The most comprehensive work in the field [23] has shown that the difference between the degree of oxidation of the cation and the calculated partial charges reflects the value of Lewis acidity. This approach was also developed further to calculate partial charge distributions in complex oxide compounds on the basis of their structural parameters [24].

It is important to note that metal oxides possess, in addition to Lewis acidity, also Brønsted acidity, defined as the ability to protonate bases (H^+-transfer). This type of acidity is the result of dissociative adsorption of water molecules on the oxide surface to form protons (H^+) and hydroxyl groups (OH^-). The driving force of these processes is the interaction between a Lewis acid (cation on the metal surface) and its conjugate base (the oxygen atom in a molecule of H_2O). A proton (Lewis acid), formed as a result of this dissociation, is captured and tightly binds the surface lattice oxygen atom of the metal oxide (Lewis base) while a hydroxyl group (base) is fixed to the metal cation (acid). It is the latter type of hydroxyl groups on the surface that are capable to exhibit acidic properties. The strength of acid sites is determined by the energy of deprotonation, which is fairly easy to

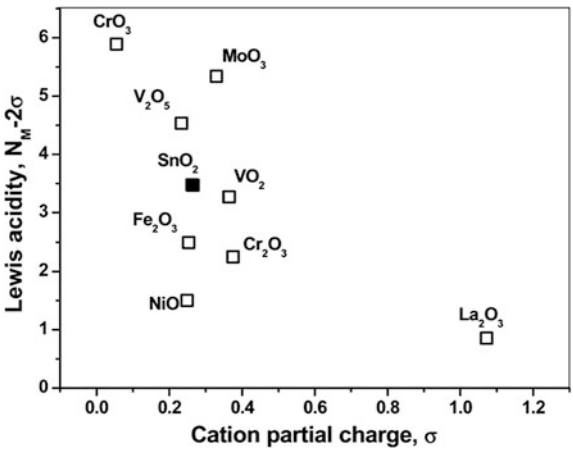

Fig. 3.3 Lewis acidity scale of simple oxides calculated on the basis of Sanderson electronegativity table [23]

quantify with the help of quantum chemical calculations [25–27]. This method is often used for catalytic materials that have shown linear correlation between the strength of Brønsted acid centers and the partial electric charges on the atoms (oxygen anions and metal cations) [24].

3.2.2 Reactivity in Oxidation Process

In most cases sensors are designed to operate in excess of oxygen in the gas phase (mainly in humid air) which means that for the majority of molecules, adsorbed on the SnO_2 surface, the next chemical step will be the interaction with different oxygen species. They are represented as chemisorbed forms of oxygen: molecular O_2^- or atomic O^-, or lattice, oxygen on the SnO_2 surface. The former are known as highly reactive electrophilic forms of oxygen, readily interacting with almost all adsorbed molecules, while the latter, lattice oxygen, considered to be less reactive nucleophilic form of oxidant. While it is widely accepted, that the concentration of chemisorbed oxygen species is the main parameter, affecting nanocrystalline SnO_2 conductance in air, little is reported about their relative importance in the process of chemical interaction of SnO_2 with gas molecules.

3.2.2.1 Oxidation by Lattice Oxygen

Oxidation of chemisorbed molecules with lattice oxygen of the oxide material was firstly described by Mars and van Krevelen [28]. For a large number of oxide systems this mechanism has been confirmed by kinetic methods as well as using direct methods of investigation of the oxides surface structure [29–31]. This process is due to lability of nucleophilic anions, which can attack the adsorbed molecules, breaking

the existing chemical bonds in these molecules and forming the new ones. The adsorption of gas molecules, which occurs with a partial transfer of electron density to the metal cation on the surface, leads to the activation of these adsorbed species—the creation of additional centers with a partial positive charge, which later may become centers for nucleophilic attack by the anion O^{2-}, located in position of lattice oxygen of the oxide compound on the surface of the material. Newly formed molecules can re-enter the process of oxidation or desorb from the oxide surface. As a result, the surface oxide is transferred into the so-called "reduced" state, characterized by a large number of oxygen vacancies and metal cations in lower oxidation states as compared with the cations in the bulk material.

If the gas phase contains a significant amount of oxygen, then re-oxidation of surface occurs through the processes: adsorption of molecular oxygen, its dissociation, and incorporation into the position of oxygen vacancies, in accordance with the following equations:

$$O_{2(g)} \leftrightarrow O_{2(ads)} \tag{3.11}$$

$$O_{2(ads)} + e^- \leftrightarrow O^-_{2(ads)} \tag{3.12}$$

$$O^-_{2(ads)} + e^- \leftrightarrow 2O^-_{(ads)} \tag{3.13}$$

$$O^-_{(ads)} + e^- \leftrightarrow O^{2-}_{(ads)} \tag{3.14}$$

$$O^{2-}_{(ads)} \leftrightarrow O^{2-}_{lat} \tag{3.15}$$

where O^{2-}_{lat} is an anion located in position of lattice oxygen of the oxide compound on the surface of the material.

Thus there is a restoration of the original chemical state of the surface and the completion of the catalytic cycle of oxidation. Processes involving nucleophilic oxygen species can be described by the following general schemes:

$$\text{Oxidation} \quad M^{n+} - O^{2-} + R \rightarrow M^{(n-x)+} + RO \tag{3.16}$$

$$\text{Regeneration} \quad M^{(n-x)+} + (x/4)O_2 \rightarrow M^{n+} + (x/2)O^{2-} \tag{3.17}$$

The use of these schemes allowed the authors [32] to describe the activity of oxides in a catalytic cycle on the basis of thermodynamic parameters. Although such a fundamental approach has revealed the energy functions that characterize the reactivity of the oxides in Redox processes, the authors could not find parallels with the real catalytic activity of oxide compounds even in very simple transformations. The reason for the failure of this, at first glance a promising concept, was the large number of additional factors influencing the Redox processes on the oxide surface, which are not taken into account in the proposed scheme of oxidation. These factors are hard to account for in a quantitative way so they are mainly used as qualitative concepts.

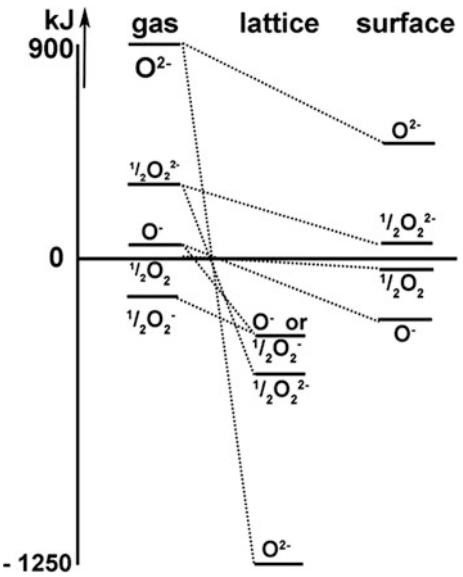

Fig. 3.4 Survey of oxygen species (From [87]. With permission.)

3.2.2.2 Oxidation via Adsorbed Oxygen

It should be taken into account that oxidation by nucleophilic lattice O^{2-} is not the only kind of oxidation reactions on the surface of oxides. The adsorption of oxygen in accordance with equations (3.11–3.14) can lead to the formation of electrophilic anions, O_2^- and O^-, on the oxide surface. The high mobility and reactivity of such species leads to oxidation processes on the surface with chemisorbed gas molecules, not subject to the "Mars-van-Krevelen" mechanism.

The nature, mechanisms of formation and chemical properties of such electrophilic oxygen anions, adsorbed on oxide surfaces, which are the subject of decade-long discussions, are still poorly known. According to the energy diagram, proposed by the authors [33], the higher the charge of the ionized forms of adsorbed oxygen, the lower its stability Fig. 3.4.

The ionized form of oxygen O_2^- in the gas phase is energetically more favorable compared to the electrically neutral molecular form. The latter can be stabilized on the oxide surface via electrostatic interaction. This chart suggests that the ionized O_2^- and O^- can exist in a mobile form on the oxide surface for a long time. The O^{2-} ion can be stabilized on the surface only in the position of the oxygen vacancy, since it is energetically very unstable species. The numerical values listed in the chart, are approximations, since they are dependent on the exact position of the ionized atoms of oxygen adsorbed on the surface, as well as their surroundings.

The ability of the oxide surface to bear chemisorbed oxygen species can only be described in a qualitative manner. For these purposes a division of oxides into three groups was proposed [34]:

The first group with a high tendency to adsorb oxygen is presented by oxides formed by the metal cations which are easily oxidized into a higher oxidation state, and therefore can easily donate electron density to the adsorbed oxygen species. A huge quantity of electrophilic anions (O^-, O_2^-) quickly form on the surface of these oxides (Examples include: NiO, MnO, CoO, Co_3O_4) at room temperature in an atmosphere with oxygen excess. With the rise of surface temperature the speed of this transformation increases considerably, and also adsorbed O^{2-} is formed, which is involved in the formation of additional lattice planes on the surface with utilization of cations, migrating from the bulk to the surface.

The second group of oxides (ZnO, TiO_2, V_2O_5, SnO_2) also possess the ability of donating electron density to the adsorbed oxygen molecules, arising primarily due to bulk non-stoichiometry within the oxygen lattice. The main difference between these two groups of oxides is the latter contains a relatively small number of active centers on the surface, through which the electron density transfer to the adsorbed oxygen molecules could pass. Formation of adsorbed O^{2-} ions is far less probable, whereas almost all the ionized particles of oxygen adsorbed on the surface are represented by O^- and O_2^-. The ability of the oxide surface to stabilize electrophilic adsorbed oxygen species may largely depend on the structural factors, namely the type of coordination environment of the metal cation and the quantity of surface oxygen vacancies. For this reason, the nature and structural features of the defects on the surface of such materials, which includes nanocrystalline SnO_2, thoroughly discussed in this chapter, can play a crucial role in the interaction of gas molecules and the subsequent sensing characteristics of metal oxide nanomaterials.

The third group of oxides is represented by compounds that do not have the ability to donate electron density to adsorbed oxygen molecules and therefore stable adsorbed electrophilic ionized forms of oxygen do not form on the stoichiometric surface of these oxides. Examples of such oxides are different molybdates, tungstates, vanadates, and other complex oxides with cations of transition elements in their highest oxidation state. Oxidation of gas molecules on their surface, as well as brief formation of adsorbed electrophilic oxygen species, can be described as a mechanism of the "Mars-Van-Krevelen"-type. Formed on the reduced surface of such oxide systems, electrophilic forms of oxygen very quickly become the nucleophilic form O^{2-}, occupying the oxygen vacancies in the crystallographic positions.

This classification is not valid for non-transition metal oxides, in which cations can exist in only a single oxidation state, and therefore do not possess electron-donor activity. The use of such oxides as heterogeneous oxidation catalysts requires extra effort to create defects in their crystal structure [34] and oxygen vacancies (F-centers) on the surface. They act as centers of adsorption and formation of electrophilic active oxygen species. Such oxides can be attributed to group II described above.

Currently, there are only a limited number of works devoted to a detailed study of the mechanisms of formation and reactivity of electrophilic forms of adsorbed oxygen on the oxide surface [35]. It is believed that these species are much more reactive than the nucleophilic lattice ions O^{2-} on the surface and have a much

greater mobility. For this reason, oxides, included in the first group mentioned above, and materials thereof, are most commonly used as catalysts for the complete and non-selective oxidation of adsorbed molecules on the surface [36]. At the same time, a clear consensus on the selectivity of oxidation processes involving electrophilic forms of adsorbed oxygen on the surface of oxides in the scientific community is currently unavailable. In some studies the role of adsorbed electrophilic O^- ions in the selective oxidation of organics is underlined [37, 38].

3.2.3 Implications for Materials Design

The synthesis of materials with well defined activity in chemical interactions with gas molecules, should be based on a theory that quantitatively describes the above mentioned considerations in clearly defined physical concepts. Such a theory so far does not exist, due to a lack of analytical techniques to examine each elementary step of interaction of adsorbed molecules on solid surfaces. These in situ experiments, including identification of the dynamic structure transformation of solid surfaces in real conditions of chemical interactions with gases, are particularly complicated in the case of oxide systems [39]. At the same time the theoretically calculated equilibrium state of the surface and molecular complexes formed on it during reaction may indeed differ from the real ones. Moreover, measurement of the kinetics of these transformations generally is beyond the capacity of modern theoretical calculations.

These reasons are responsible for the impossibility of a sensing material's design from first principle calculations. Thus, the theoretical basis for the development of new oxide materials with improved properties in Redox reactions (higher activity and/or selectivity)—is still a huge accumulated empirical experience, combined with the qualitative concepts of reactivity given above. Therefore, one of the possible approaches for a partially directed synthesis of new oxide materials is a modification of the existing oxide systems by the introduction of additives [40]. Such modifiers may occupy different positions, both on the surface of the material and in its structure, providing a complex effect on its activity in interaction with the gas phase [41]. Depending on the concentration and type of introduced additional components, they can form solid solutions based on the main phase or create a segregation of the modifier on the surface of crystalline grains of the main phase. In some cases the stabilization of thermodynamically unstable phases can be observed. So, the modifiers cause changes in the parameters of the crystal structure itself, as well as in related properties (for example energy and length of the metal–oxygen bond), and also change the concentration of point defects, both in the cation and anion sublattices. Being distributed on the surface, these additives can also change the local structure and properties of active sites, through formation their own two-dimensional oxide structure and thus "block" the pre-existing active sites.

To check the validity of the proposed approach to selected modifiers that provide increased sensitivity and selectivity of tin dioxide towards gases of

different chemical nature, we experimentally examined the modifiers with variable acid–base properties and activity in the oxidation process such as noble metals and metal oxides: Au, PdO_x, RuO_2, NiO, CuO, Fe_2O_3, La_2O_3, V_2O_5, MoO_3, Sb_2O_5.

3.3 Influence of Modifiers on SnO_2 Surface Acidity

Thermoprogrammed desorption of ammonia (TPD–NH_3), along with methods of microcalorimetry and IR spectroscopy is one of the most commonly used methods to assess the acidity of the surface—the strength and the concentration of both Lewis and Brønsted centers. The number of acid sites and their distribution over the activation energy of desorption of ammonia can be carried out using a model [42] with the assumption that one molecule of NH_3 desorbs from a single acid site.

For most of the materials, discussed in this chapter, two types of adsorption sites on the surface, possessing different acidity, were found—weak ($T_{des} \sim 120$ °C) and strong ($T_{des} \sim 480$ °C) (Fig. 3.5). Weak acid–base interaction of NH_3 with the material's surface corresponds to the Brønsted acidity centers—the hydroxyl groups on the surface which formed partly due to the adsorption and dissociation of molecular water from the air. It is reasonable, however, to judge that the number of these hydroxyl groups is governed by the heat treatment conditions of the precursor—α-stannic acid [43]. Complete removal of water is achieved at temperatures above 600 °C, which is reflected in a gradual decrease in the desorption peak in the spectra of TPD-NH_3 at 120 °C, (Acquisition of this TPD followed the sample pretreatment for 1 h at 300 °C in dry air with subsequent cooling down to room temperature in same gas flow; saturation with 10 % NH_3 in N_2 for 0.5 h and further TPD in a N_2 flow), for materials based on pure tin dioxide produced by higher annealing temperatures in an air atmosphere. Strong adsorption sites are coordinatively unsaturated metal cations on the surface of materials, which have the capacity to interact with Lewis bases due to unfilled positions in an oxygen coordination. There are two types of such cations on the surface—Sn^{4+} with 5 oxygen atoms in the coordination sphere and Sn^{2+} with 4 oxygen atoms in the anion environment. In this case, cations Sn^{2+}_{4c} have greater bond strength with adsorbed NH_3 molecules due to the additional contribution of covalent interactions [44]. Displacement of the TPD-NH_3 maxima at higher temperatures with increasing annealing temperature is probably due to the effects of long-range order, manifested in a decrease in the degree of crystal lattice defects on the surface of the grains. For this reason, a valid comparison between Brønsted and Lewis acidity of the surface of modified materials with each other is only possible for substances produced using the same annealing temperature and with the same annealing gas conditions. Concentrations of Brønsted and Lewis acid sites for the materials under discussion are presented in Table 3.1.

Introduction of modifiers with lower optical basicity (higher Lewis acidity of cations) to the SnO_2 matrix and vice versa is accompanied, as in the case of Brønsted acid centers, with the corresponding change in their concentration on the surface (Fig. 3.6). We emphasize that such a law is valid only for materials with

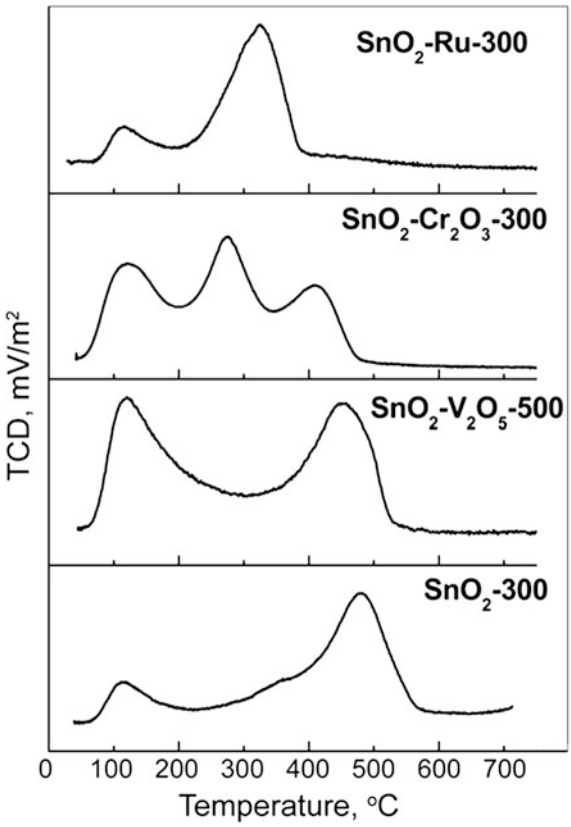

Fig. 3.5 Examples of TPD-NH_3 spectra of SnO_2-based sensor materials

the same thermal treatment, indicating the decisive contribution of crystal lattice defects on the surface in the amount of acid sites.

For a number of materials (SnO_2–Cr_2O_3, SnO_2–Pd and SnO_2–Ru) the desorption peak at about 300 °C instead of 480 °C was observed. One can attribute the peaks at 300 °C not to the desorption of ammonia, but to the products of NH_3 dissociation and oxidation (molecular nitrogen or nitrogen oxides). This is due to pronounced catalytic activity of deposited clusters of noble metals, manifested in many oxidation reactions of adsorbed molecules with oxygen. Also the possibility to create the additional chromyl oxygen anions (Cr = O) on the surface of Cr_2O_3, actively involved in the oxidation of adsorbed molecules [45, 46], may be the reason of such NH_3-TPD dependencies in the case of Cr-modified SnO_2.

Table 3.1 Parameters of SnO_2-based semiconductor sensor materials

Sample[a]	T_{an} ◦C	d_{XRD}, nm	S, m^2/g	Brønsted acidity, μmol NH_3/m^2	Lewis acidity, μmol NH_3/m^2
SnO_2-300	300	4	65	0.554 ± 0.05	3.1 ± 0.3
SnO_2-500	500	9	27	0.147 ± 0.01	1.58 ± 0.2
SnO_2-700	700	13	15	0.135 ± 0.01	1.03 ± 0.1
SnO_2-Fe_2O_3-500	500	5	40	0.385 ± 0.04	3.73 ± 0.4
SnO_2-V_2O_5-500	500	6	42	1.56 ± 0.15	7.05 ± 0.7
SnO_2-Cr_2O_3-500	500	9	40	1.64 ± 0.16	–
SnO_2-MoO_3-500	500	5	75	0.915 ± 0.09	2.22 ± 0.2
SnO_2-Cr_2O_3-300	500	4	114	1.11 ± 0.1	–
SnO_2-Pd-500	500	8	27	–	–
SnO_2-Pd-300	300	4	61	0.633 ± 0.06	–
SnO_2-Au-300	300	4	60	0.188 ± 0.01	1.96 ± 0.2
SnO_2-NiO-Au-350	350	5	75	0.457 ± 0.05	1.86 ± 0.2
SnO_2-Pt-500	500	13	15	0.673 ± 0.07	–
SnO_2-Ru-300	300	5	67	0.334 ± 0.03	–
SnO_2-Ru-700	700	20	13	–	–
SnO_2-La_2O_3-700	700	5	27	0.032 ± 0.03	1.53 ± 0.2
SnO_2-CuO-700	700	13	15	–	–
SnO_2-Sb-300	300	4	71	0.76 ± 0.08	2.33 ± 0.2

[a] Sample naming: Base material-Modifier-Calcination temperature

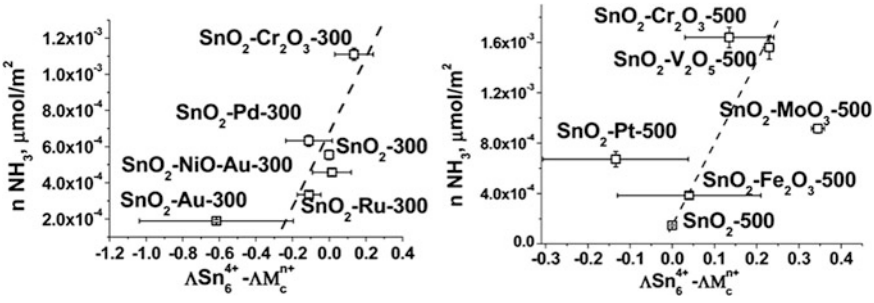

Fig. 3.6 Density of brønsted-type acid sites on the surface of differently modified nanocrystalline SnO_2 calcined at 300 °C (*left*) and 500 °C (*right*)

3.4 Redox Properties of Modified Materials

3.4.1 Chemisorbed Oxygen

Information regarding the Redox properties of surface modified tin dioxide can be obtained by the in situ investigation of a material's interaction with oxygen and temperature-programmed reduction within a H_2 environment.

The dependence of the SnO_2 electrical conductivity on oxygen partial pressure was investigated in detail in a wide temperature range [47, 48]. The electrical behavior of these semiconductor oxides at low temperatures is controlled by acceptor impurities—various species of chemisorbed oxygen. At 200 – 400 °C the interaction of atmospheric oxygen with an n-type semiconductor oxide surface leads to the formation of molecular (O_2^-) and atomic (O^-, O^{2-}) chemisorbed species. In general, the oxygen chemisorption can be described as [49]:

$$\frac{\beta}{2} O_{2(gas)} + \alpha \cdot e^- + S \leftrightarrow O^{-\alpha}_{\beta(ads)}, \tag{3.18}$$

where $O_{2(gas)}$ is an oxygen molecule in the ambient atmosphere, e^- is an electron, which can reach the surface, meaning it has enough energy to overcome the electric field resulting from the negative charging of the surface. Their concentration is denoted as n_S; $n_S = [e^-]$; S is an unoccupied site or other surface defects suitable for oxygen chemisorption; $O^{-\alpha}_{\beta(ads)}$ is a chemisorbed oxygen species with $\alpha = 1$ and 2 for a singly and doubly ionized forms, $\beta = 1$ and 2 for atomic and molecular forms respectively.

Following the reasoning presented by authors [50] and considering the Weisz limitation [50], one can obtain

$$\lg n_S = const' + \lg\left(1 - \frac{n_S}{n_b}\right) - m \lg p_{O_2} \tag{3.19}$$

where n_b is the concentration of charge carriers in the bulk, m = 1, 0.5, or 0.25 for O_2^-, O^- and O^{2-} respectively.

If the sensing element is a porous film formed by small grains with grain size $d_{XRD} < 50$ nm, complete grain depletion and a flat band condition can be expected [50] and the conductivity is proportional to n_S. Thus, Eq. (3.19) can be presented as:

$$\lg G = const1 + \lg\left(1 - \frac{G}{G_0}\right) - m \lg p_{O_2} \tag{3.20}$$

In this case G is the material conductivity at the given partial oxygen pressure, G_0 – material conductivity at $p_{O_2} \to 0$. Taking G_0 to be equal to the material conductivity under an inert atmosphere (for example in pure Ar, containing no more than 0.002 vol. % O_2), it is possible to determine experimentally the value of $\lg\left(1 - \frac{G}{G_0}\right)$ for any fixed p_{o_2}. If the experimental plots of G vs. p_{o_2} in coordinates

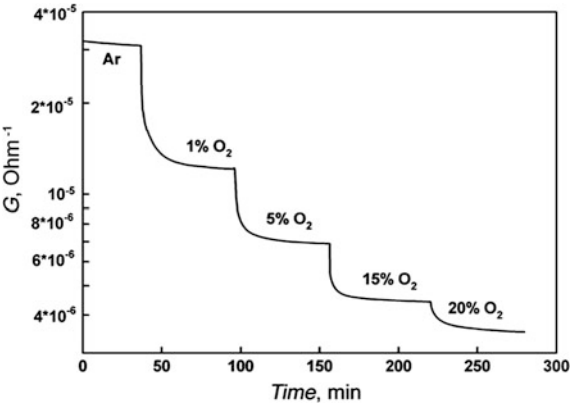

Fig. 3.7 Conductivity of SnO_2-500 sample at step-by-step increase of oxygen partial pressure at 400 °C

$\left(\lg G - \lg\left(1 - \frac{G}{G_0}\right)\right)$ against $(\lg p_{O_2})$ are linear, one can determine from the curve slope the predominant form of chemisorbed oxygen [51].

For pure and chemically modified SnO_2 the reversible decrease in electrical conductivity G is observed with increasing the partial pressure of oxygen in the gas phase (Fig. 3.7). The values of G for a fixed partial pressure of oxygen can be used for the analysis of the $\left(\lg G - \lg\left(1 - \frac{G}{G_0}\right)\right)$ against $(\lg p_{O_2})$ dependence in the temperature range 200–400 °C. In the coordinates corresponding to Eq. (3.20), the obtained dependencies of conductivity vs. oxygen partial pressure are linear (Fig. 3.8). That allows us to determine the coefficient m in the equation for the slope and to suppose the predominant form of chemisorbed oxygen. Thus, the values of $m = 1$, 0.5 and 0.25 suggest that the predominant form is $O^-_{2(ads)}$, $O^-_{(ads)}$ *and* $O^{2-}_{(ads)}$ respectively. The calculated values of m for unmodified SnO_2 are summarized in Table 3.2.

At T = 200 °C oxygen chemisorption on SnO_2 surface proceeds mainly with formation of the molecular $O^-_{2(ads)}$ form ($m \approx 1$). A decrease of m with the temperature increase points to an increase in the amount of atomic $O^-_{(ads)}$. With the increase of SnO_2 grain size this effect becomes more significant.

At T = 200 °C the introduction of modifiers does not affect the type of the predominant form of chemisorbed oxygen. Thus, the chemisorption of oxygen at this temperature occurs mainly with the formation of the molecular form, regardless of the type of modifier. For higher temperatures, the value of m decreases for the modified tin dioxide, which indicates an increasing contribution of atomic $O^-_{(ads)}$ form (Fig. 3.9).

The observed trend in increasing the influence of modifiers on the type of the predominant form of chemisorbed oxygen in the series Fe < In < La < Ru < Ni < Au < Pd < Pt can be due to a combination of several factors. The formation of a monatomic form of chemisorbed oxygen can occur in dissociative adsorption (reaction (3.11–3.15)), as well as due to the decomposition of unstable

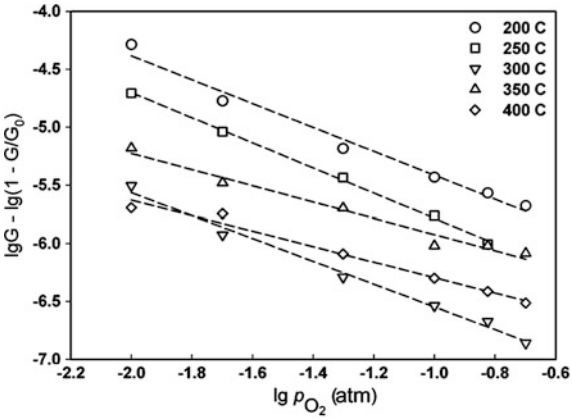

Fig. 3.8 Conductivity of SnO_2-500 ($d_{XRD} = 14$ nm) vs. oxygen partial pressure in coordinates of Eq. (3.20)

Table 3.2 Calculated values of coefficient m for unmodified SnO_2

d_{XRD}, nm	*m*				
	200 °C	250 °C	300 °C	350 °C	400 °C
4	0.98 ± 0.05	1.03 ± 0.02	1.02 ± 0.05	1.02 ± 0.03	0.80 ± 0.04
14	1.03 ± 0.07	1.03 ± 0.03	0.98 ± 0.05	0.88 ± 0.06	0.69 ± 0.05
28	0.94 ± 0.05	1.05 ± 0.02	1.02 ± 0.05	0.70 ± 0.06	0.67 ± 0.06
43	–	0.94 ± 0.03	0.89 ± 0.05	0.68 ± 0.09	0.65 ± 0.03

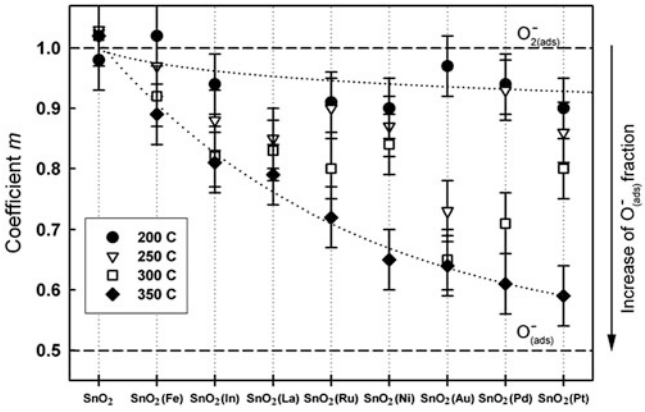

Fig. 3.9 Influence of modifier on the oxygen chemisorption on SnO_2 surface

molecular form$O^{2-}_{2(ads)}$ that can be formed by the localization of the second electron on molecular $O^{-}_{2(ads)}$ ion:

$$O^{-}_{2(ads)} + e^{-} \leftrightarrow O^{2-}_{2(ads)}. \tag{3.21}$$

Table 3.3 Distribution of oxides between the groups [5] in accordance with *qo* dependence on $\Delta\chi$ value

Group					
I		II		III	
Oxide	*qo*	Oxide	*qo*	oxide	*qo*
RuO_2	−0.74	SnO_2	−0.86	La_2O_3	−1.08
PdO	−0.89	Fe_2O_3	−0.87		
PtO_2	−1.00	In_2O_3	−0.87		
		NiO	−1.02		

Thus, the conditions of $O^-_{(ads)}$formation may be the dissociation of oxygen (reaction (3.13)) or increase of negative charge on the adsorbed molecular oxygen species.

The authors of review [5] showed that, depending on the ratio of the charge *qo* of the lattice oxygen atom and the difference in electronegativities of elements $\Delta\chi$, crystalline oxides can be generally divided into three groups. The first group includes oxides of platinum metals. For this group of oxides, the minimum value q_O from −0.8 to −1.0 is typical. The second group includes oxides of p-and d-elements, and uranium oxides. The charge of oxygen varies in the range q_O from −0.6 to −1.3. The third group consists of oxides of alkali, alkaline earth and rare earth elements. This group can be characterized by the highest negative charge of oxygen q_O from −1.0 to −1.9 and the maximum $\Delta\chi$ value. In all groups, the negative charge of oxygen decreases with $\Delta\chi$ increasing.

Tin dioxide and oxides of the above modifiers can be assigned to the groups described in Table 3.3. Within each group the increase of negative charge on the oxygen anions within the modifier oxide results in the growth of oxygen chemisorbed on the surface of nanocrystalline SnO_2 as the atomic ion, $O^-_{(ads)}$. Thus, the partial charge on oxygen in the corresponding modifier oxide can be used as a criterion for assessing the ability of the cation to the transfer of electron density to oxygen.

At the same time, with similar values *qo*, the modifiers of group I have the greatest influence on the chemisorption of oxygen. Probably, this may be due to the fact that clusters of platinum metals and their oxides additionally catalyze the dissociation of oxygen molecules by reaction (3.13), which leads to a significant increase in the atomic form of chemisorbed oxygen. The high activity of platinum group metals in this process is shown earlier in experiments on isotopic exchange of oxygen O^{16}/O^{18} [52, 53] in oxides SiO_2, Al_2O_3, ZrO_2, TiO_2.

Oxygen adsorption on gold particles occurs without dissociation [54]. Thus, the mechanism of the effect of gold on the dominant type of particles of chemisorbed oxygen differs from that discussed above. Adsorption of oxygen on the surface of heterocontact Au/SnO_2 was studied by the authors [55] through electrical conductivity and calorimetry measurements. It was found that the heat of oxygen adsorption on the Au/SnO_2 is significantly higher than the corresponding values

obtained for the adsorption of O_2 on the SnO_2 and Au separately. It was suggested that at the interface gas—Au–SnO_2 there are forms of chemisorbed oxygen with a higher negative charge compared with the species chemisorbed on the surface of the unmodified oxide. The mechanism proposed in [56], includes the exchange of electrons between the Au and SnO_2. Thus, one can assume that the formation of oxygen particles on the Au/SnO_2 occurs through an intermediate stage of formation of unstable molecular $O^{2-}_{2(ads)}$ forms.

Overall, the observed tendency to increase the fraction of atomic form of chemisorbed oxygen is in a good agreement with the increase of optical basicity or decrease of Lewis acidity of the cations of modifiers (Fig. 3.10). Thus, these approaches can be used for the qualitative prediction of the influence of modifiers on the oxidative activity of oxygen chemisorbed on SnO_2 surface.

3.4.2 Temperature Programmed Reduction by H_2

Hydrogen consumption during TPR-H_2 (preannealing at 300 °C in dry air with further cooling in the same flow, followed by TPR in 5 % mixture of H_2 in Ar) goes through two pronounced maxima, the first of which is in the low temperature range of 100–350 °C, while the second, more pronounced - in the high temperature range 380–660 °C (Fig. 3.11). High-temperature maximum corresponds to the hydrogen absorption during reduction of material to metallic tin, the low-temperature one reflects the absorption of hydrogen by chemisorbed oxygen species and the terminal atoms of the lattice oxygen on the surface of SnO_2. This process, called "reduction of the surface", results in an increase of the number of lattice oxygen vacancies in the positions of the bridging oxygen, and the proportion of cations Sn^{2+}_{4c} on the surface. The presence of the shoulder in the high-temperature peak of hydrogen consumption reflects the transition of tin dioxide SnO_2 into SnO, followed by full reduction to metallic tin. Reduction to an intermediate state is ensured by reaction with surface O^{2-}anions among the total number of oxygen atoms in the lattice. With increasing SnO_2 grain size, the fraction of surface oxygen atoms is sharply reduced, as evidenced by the decrease in the low-temperature peak for hydrogen consumption. At the same time the shoulder on high-temperature peak almost disappears and becomes shorter, indicating that the processes of reducing the tin dioxide matrix to SnO and then to metallic tin occur in parallel.

For materials modified with Ru, Pt and, in particular, Pd, the high-temperature hydrogen consumption maximum shifts toward lower temperatures (Fig. 3.12). This may be caused by the catalytic activity of noble metal clusters in the matrix of nanocrystalline tin dioxide. The most likely mechanism is a joint spillover of hydrogen and oxygen on the SnO_2 crystal lattice through the PdO_x clusters [56]. Reduction of SnO_2 at a lower temperature becomes possible due to the dissociation of hydrogen molecules on Pd or PdO_x clusters. Examples illustrating this

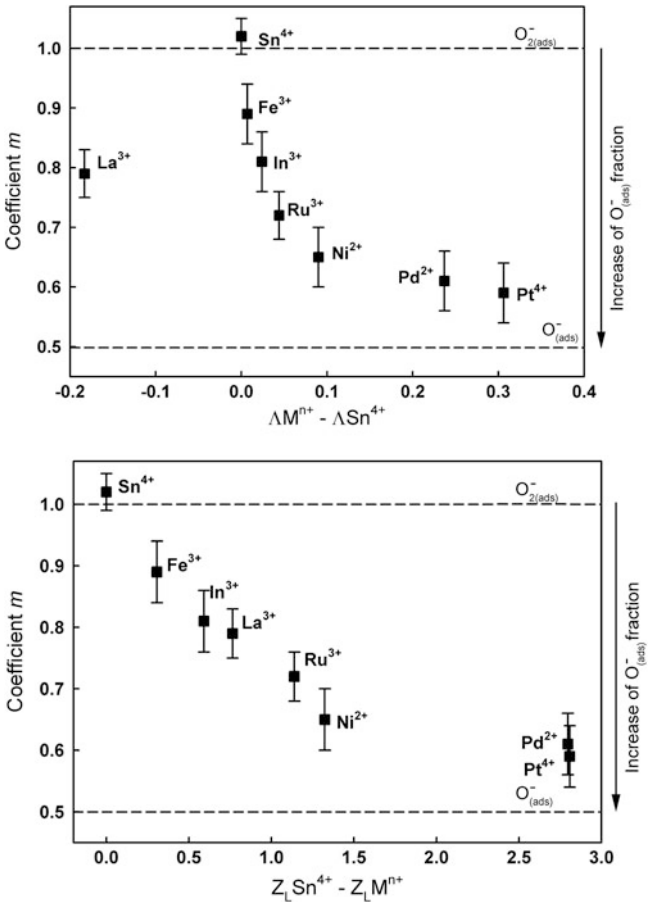

Fig. 3.10 The relationship between nanocrystalline SnO_2 surface modifier Lewis acidity, defined in terms of optical basicity (*top*) and Zhang electronegativity (*bottom*), and ratio between different forms of adsorbed oxygen

mechanism of interaction with the gas phase for systems Rh/TiO_2, Rh/Al_2O_3, Rh/CeO_2, Rh/SiO_2, Pt/Al_2O_3, Pd/Al_2O_3, Pd/Mn_2O_3, are presented in the review [57]. The onset of high temperature maxima, representing hydrogen consumption, for other materials is manifested nearly at the same temperature ($\sim$420 °C), which indicates the energy barrier for Mars van Krevelen oxidation of adsorbed molecules [57].

For pure SnO_2 with small crystallite size of 4 nm the amount of chemisorbed oxygen estimated from TPR-H_2, assuming the interaction

$$O^-_{2(ads)} + 2H_2 = 2H_2O + e^- \tag{3.22}$$

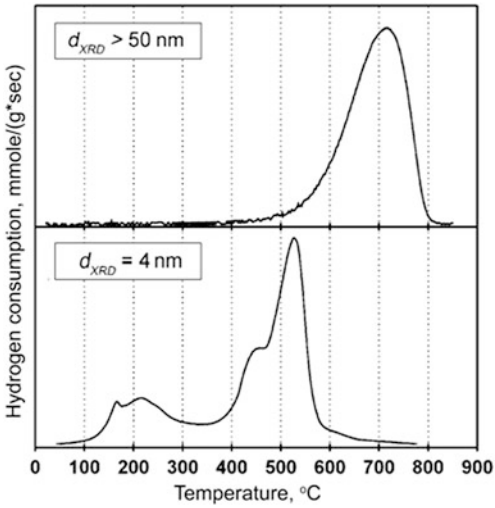

Fig. 3.11 Typical TPR spectra for unmodified SnO_2 with different crystallite size d_{XRD}

is $\sim 5 \times 10^{-6}$ mol/m^2 or 5×10^{-2} of monolayer. According to Weisz limitation [51], this quantity corresponds to the upper boundary of the coverage density of the semiconductor surface by charged particles in equilibrium conditions.

In most cases surface modification of tin dioxide leads to a decrease of hydrogen consumption at low temperatures. This may be indirect evidence of increasing the atomic anionic form of chemisorbed oxygen on the SnO_2 surface (see Fig. 3.9). In fact, if one compares the reaction (3.22) and

$$O^-_{(ads)} + H_2 = H_2O + e^- \tag{3.23}$$

for the surfaces with the same negative charge caused by oxygen acceptor species the hydrogen consumption is less in the latter case. However, comparing the amount of consumed hydrogen and the part of atomic form of chemisorbed oxygen for tin dioxide modified with various catalysts, does not show unequivocal correlations. The decrease in the total amount of chemisorbed oxygen may be additionally due to blockage of adsorption centers by the cations of modifiers. It is impossible to take into account this factor quantitatively because of the complicated distribution of modifiers between surface and bulk of SnO_2 crystallites.

Analysis of the concentration of highly reactive oxygen species on the surface of materials can be done by TPR-H_2 after pre-treatment in different atmospheres (Fig. 3.13). Annealing in nitrogen flow at 300 °C for 1 h, in contrast to the pre-treatment in synthetic air under the same conditions, is intended to remove weakly bonded forms of chemisorbed oxygen from the surface. The chemical inertness of nitrogen allows exclusion of the possible surface reduction in the chemical reaction. At the same time, desorption of mobile oxygen species from the surface is sustained due to the fact that the nitrogen molecule has a polarizability close to that of molecular oxygen. This property makes the N_2 molecule competitive in the process of adsorption at the centers occupied by chemisorbed oxygen particles [34].

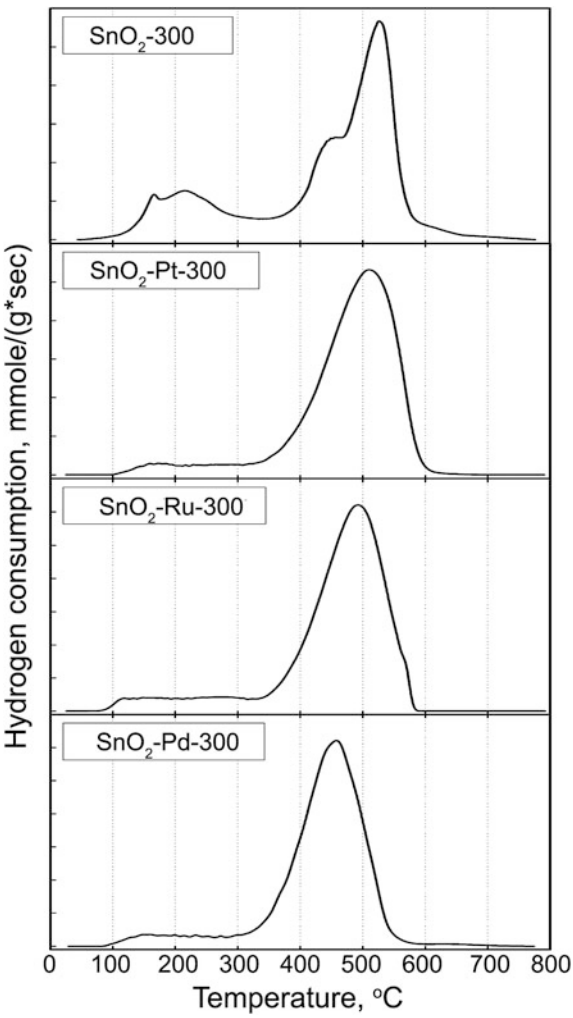

Fig. 3.12 TPR spectra of SnO_2-based sensor materials

The decrease of low-temperature peak of hydrogen consumption after sample pre-treatment in nitrogen indicates the desorption of mobile forms of chemisorbed oxygen. The difference of TPR-H_2 spectra, taken under different pre-treatment conditions, allows us to estimate the concentration of these oxygen species on the surface of materials (Fig. 3.14).

For the samples, obtained in the same conditions, the maximum concentration of mobile oxygen species is observed for materials modified with Cr_2O_3 and PdO_x. In both cases a likely explanation may be explained via the chemical oxidation of the modifier in an air atmosphere to the higher oxidation state. In the former case the oxidation goes through formation of chromyl group Cr = O and at least partial oxidation of metallic Pd clusters to PdO in the latter. Both materials are presumed

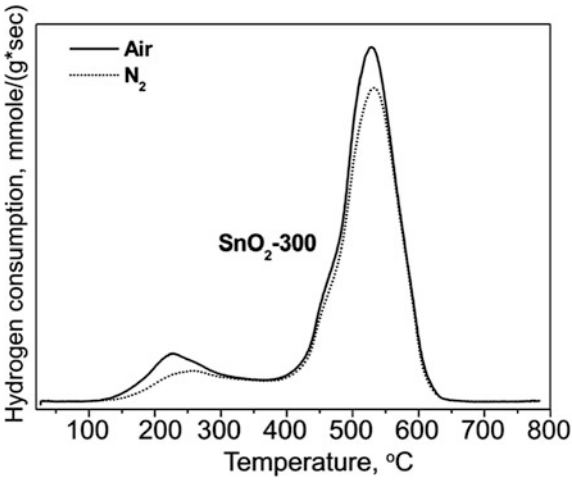

Fig. 3.13 TPR-H_2 spectra of SnO_2-300 material evaluated after sample pretreatment in different gas atmospheres

thus to be especially active in the surface oxidation processes. Overall the introduction of modifiers leads in general to a slight increase in adsorbed oxygen content, perhaps due to the introduction of additional point defects on the surface acting as additional adsorption and dissociation sites for oxygen molecule.

3.5 Classification of Gases

Properties of certain molecules: first ionization potential, electron affinity, proton affinity, which have an impact on the nature of their interaction with the surface of a semiconducting oxide, are shown in Fig. 3.15 [58]. The compounds are grouped in order of increasing proton affinity and reducing first ionization potential.

A pre-selection of the modifier to create a selective sensing material can be made on the basis of analyzing the properties of gas molecules to be detected. Target gases can be divided into groups as shown in Fig. 3.15 based on the mode of interaction with the semiconductor oxide surface. First it is necessary to distinguish oxidizing (electron accepting) and reducing (electron donating) ones. Gases should be considered as oxidizing agents when their adsorption on the surface leads to a decrease in charge carrier concentration in the surface layer of n-type semiconductor oxides due to electron capture. This group includes gas molecules with high electron affinity and high ionization potential (Group I, Fig. 3.15): oxygen, nitrogen dioxide, ozone, chlorine.

The reducing agents are gases, for which the interaction with the surface of n-type semiconductor oxide results in an increase of the charge carrier concentration in the surface layer of the latter. This effect is caused by oxidation of the reducing gas molecules by oxygen chemisorbed on the oxide‘s surface or lattice oxygen as it is described in the previous paragraph. This mechanism of a change in charge carrier

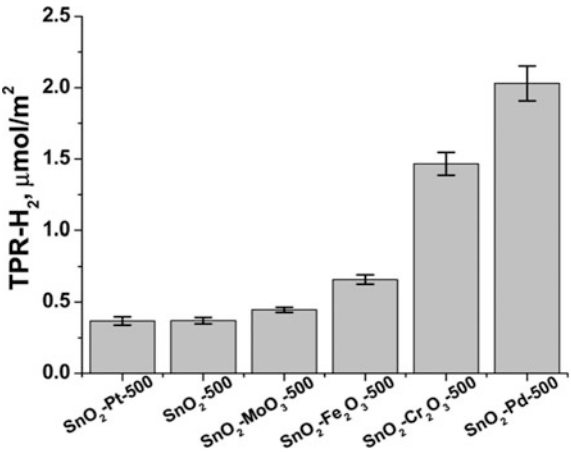

Fig. 3.14 The amount of hydrogen, consumed by mobile adsorbed oxygen forms on the surface of SnO_2-based sensor materials

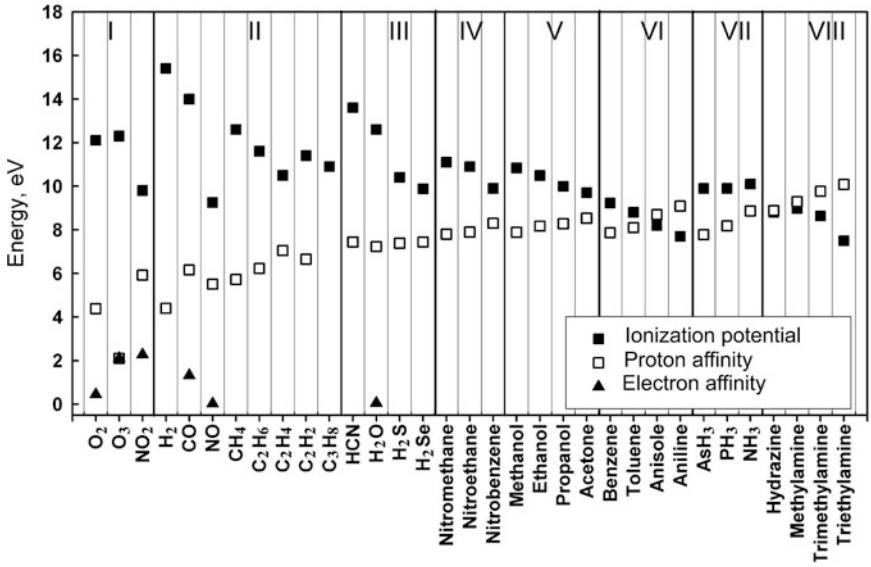

Fig. 3.15 Classification of gases

concentration is typical, especially, in the oxidation of gases that do not possess pronounced electron-donor properties and have low proton affinity: CO, H_2, saturated hydrocarbons (Group II, Fig. 3.15). In contrast, the reactions of gas molecules having pronounced acidic (Group III, Fig. 3.15) or basic (Groups VII, VIII, Fig. 3.15) properties with the surface of sensitive material may include an interaction of the donor-acceptor mechanism in addition to oxidation. The reactions of complex organic molecules containing various functional groups (Groups IV–VI, Fig. 3.15), on the surface of a semiconductor oxide can proceed via different routes, depending

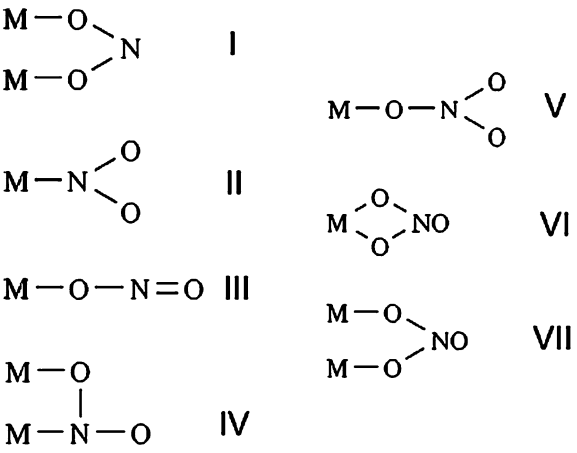

Fig. 3.16 Various NO_2 derived species, formed on oxide surface

on the concentration of basic and acid adsorption centers of different strengths on the surface of the semiconductor.

In Sects. 5.1–5.5 these principles will be discussed in more detail. Specific attention will be paid to material and chemical characteristics which lead to a general selection of sensor materials (and modifiers) for detection of typical representatives of the different groups of gases mentioned above—NO_2 (Group I), CO (Group II), NH_3 (Group VII), H_2S (Group III), and acetone vapor (Group V). Section 6 will highlight the sensor operating characteristics of the selected sensor materials (and modifiers) towards these specific target gases.

3.5.1 Oxidizing Gases: NO_2

Interaction of NO_2 molecules with the surface of oxides can proceed by the mechanism of molecular and dissociative adsorption. In the first case the formation of various nitrite (NO_2) and nitrate (NO_3) surface groups [59] is possible (Fig. 3.16)

Numerous literature data provide evidence that the interaction of n-type semiconductor oxides with NO_2 is accompanied by a decrease in electrical conductivity, i.e., like oxygen, nitrogen dioxide is an electron acceptor. Thus, the interaction of NO_2 with surface centers—Lewis acids with the formation of nitronium ion (Fig. 3.16b)

$$NO_2 + M^{n+} \rightarrow NO_2^+ + M^{(n-1)+} \tag{3.24}$$

can not be responsible for changing the electrical conductivity of materials.

The electron affinity of NO_2 molecule is 2.27 eV [60], which considerably exceeds the analogous value for the oxygen molecule (0.44 eV [61]). This determines the possibility of detecting low concentrations of NO_2 in the air in the

presence of ~20 vol. % of oxygen. Authors [62] using Raman spectroscopy showed that the electrical conductivity of SnO_2 in the presence of NO_2 correlates with the concentration of surface bidentate nitrite group. Ab initio calculations [63] indicate that the most energetically favoured is the molecular adsorption of nitrogen dioxide with the coordination of one or both of the oxygen atoms of NO_2 molecules on the vacancies of bridging oxygen atoms on a partially reduced surface of tin dioxide.

Study by infrared spectroscopy and programmed desorption in the temperature range 25–400 °C [64] showed the possibility of dissociation of NO_2 during interaction with the surface of tin dioxide. The presence of NO in the thermal desorption products can serve as indirect evidence of the occurrence of following reactions:

$$NO_{2(gas)} \leftrightarrow NO_{2(ads)}, \tag{3.25}$$

$$NO_{2(ads)} + e^- \leftrightarrow NO^-_{2(ads)}, \tag{3.26}$$

$$NO^-_{2(ads)} \leftrightarrow NO_{(gas)} + O^-_{(ads)}. \tag{3.27}$$

To increase the SnO_2 sensor signal towards NO_2 it seems to be reasonable to introduce electron donor modifiers that increase the concentration of electrons with sufficient energy to overcome the barrier created by the negatively charged surface. Alternatively the use of modifiers that are able to transfer electron density to the oxygen belonging to the acceptor chemisorbed species through an increase in the degree of oxidation should also enhance the sensing signal towards NO_2.

3.5.2 Reducing Gases: CO

The mechanism of CO interaction with the surface of metal oxides depends primarily on temperature. Since the CO molecule can act as both the donor and acceptor of electrons, it can react with acidic surface centers—coordinatively unsaturated metal cations (Lewis acids) and oxygen ions, which have basic properties according to acid–base classification, given by Lewis. At low temperatures, CO adsorbs on metal cations. The structure of the molecular orbitals of CO is that the electron density transfer is possible from both the CO molecule to the free orbital of the metal (σ-donor), and vice versa—from the d-orbitals of the metal to unoccupied antibonding orbitals of CO (π-acceptor) [60]. At elevated temperatures carbon monoxide on the surface of oxide reacts with chemisorbed oxygen species or with oxygen anions in the crystal lattice. The final product of oxidation is CO_2.

The main reaction responsible for sensor signal generation, is namely the oxidation of CO by chemisorbed oxygen. Therefore, modifiers that increase the concentration and mobility of oxygen species on the surface of SnO_2, are of greatest interest for the development of highly sensitive materials for CO detection.

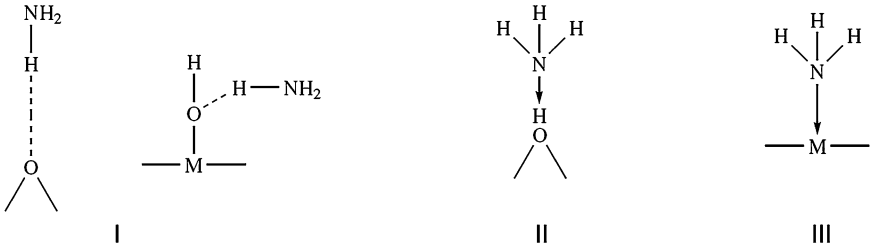

Fig. 3.17 Scheme of possible ammonia coordination on oxide surface

3.5.3 Reducing Bases: NH_3

Ammonia molecules can adsorb on the oxide surface through formation of hydrogen bonds with surface atoms of oxygen or oxygen from hydroxyl groups (Fig. 3.17a), a hydrogen bond between the nitrogen and hydrogen of the hydroxyl group (Fig. 3.17b) or a coordinative donor-acceptor bond with an unsaturated surface metal cation (Fig. 3.17c) [60]:

The formation of NH_4^+ ion is a criterion for the presence of surface Brønsted acid centers—hydroxyl groups, whereas the coordination of the NH_3 molecules indicates the presence of Lewis acid centers. Dissociative adsorption of ammonia leads to the formation of NH_2-and OH-groups on the surface:

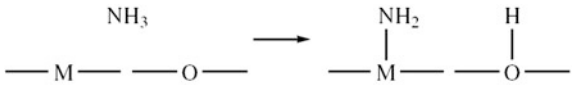

(3.28)

Based on the presented data one can suggest that the increase in NH_3 adsorption on the surface of tin dioxide and, possibly, enhancement of sensor response can be achieved by increasing the number of acidic adsorption sites.

3.5.4 Reducing Acids: H_2S

Interaction of gaseous hydrogen sulfide with the oxide surface is characterized by two factors. First, hydrogen sulfide is a strong reducing agent: the value of the ionization potential of the H_2S molecule is 4.10 eV. Secondly, hydrogen sulfide is a Brønsted acid, i.e. heterolytic cleavage of the S–H bond is quite easy, especially via the formation of new donor-acceptor bonds. Thus, H_2S can interact with various centers on the oxide surface (Fig. 3.18) [60]:

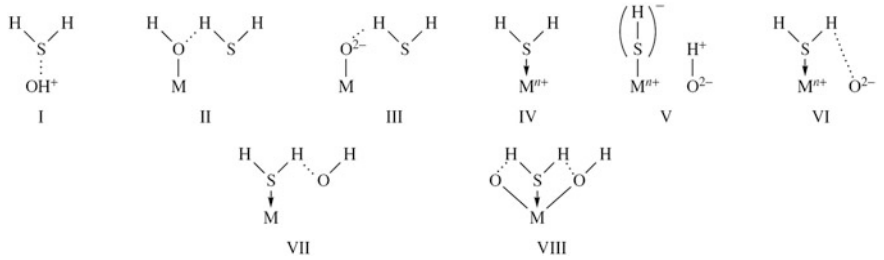

Fig. 3.18 Scheme of possible H_2S coordination on oxide surface

The possible reactions are [60]:

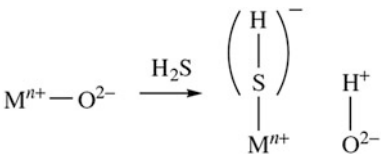

(3.29)

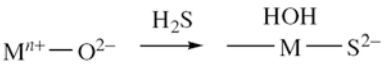

(3.30)

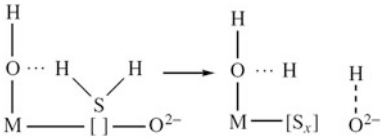

(3.31)

$$M^{n+}O^{2-} + H_2S \rightarrow [S_\chi] + M^{(n-2)+} + H_2O \tag{3.32}$$

As a result of interaction with gaseous hydrogen sulfide the following changes were found at the oxides surface [60]:

- formation of sulfides;
- partial blocking of Lewis acid sites;
- reduction of metal cations with variable valence;
- oxidation of sulfur and increasing acidity of the surface through formation of SO_x groups.

An increase in H_2S adsorption on the surface of tin dioxide can be achieved with the introduction of modifiers that increase the electron-donor ability of surface basic centers (oxygen anions). In this case the H_2S adsorption is accompanied by heterolytic reaction with the Lewis acid/base pair on the oxide surface. The maximum augmentation of sensor signal is possible if the interaction of a high-resistance modifier oxide with hydrogen sulfide results in the reversible formation of a highly conducting sulfide.

3.5.5 Complex Organics: Acetone

Acetone represents a complicated case for gas sensing since it can interact with metal oxide surfaces via a number of reaction routes. Each of these mechanisms for sorption affects further transformation steps, so there are number of products expected to form prior to desorption. In this sense the assumption, that the conversion of organic molecules to CO_2 and H_2O is the process, which solely governs the sensor response, seems to be an oversimplification. The polar carbonyl group is a moiety, which in the first step, could take part in the adsorption on a metal oxide surface. According to IR data it usually goes through formation of an enol species [65, 66] with further dissociation and formation of propene-2-olate strongly bonded to the surface metal cation and a proton bound to surface oxygen with the formation of a hydroxyl group. This transformation may lead to acrolein or acrylic acid. At the same time the highly electrophilic carbonyl carbon atom may be attacked by nucleophylic O^{2-} with further carbon chain cleavage and partial oxidation to acetic acid [67] or acetic aldehyde. It was shown also that the condensation of two nearby adsorbed enolates gives rise to complex molecules (oxidative coupling) [66, 67]. The interaction of adsorbed enolate with Brønsted acid sites may give a dehydration product—propene—and water as a result of the slight Brønsted basicity of the enol group. The ratio of these reaction rates at the solid surface is governed mainly by surface cation acidity and anion basicity and may be shifted to either of the processes via surface modification [37].

Also the interaction of adsorbed organic molecules with highly reactive electrophilic adsorbed oxygen species should be taken into account. It is generally referred to as an unselective interaction, giving rise to a number of products of partial oxidation or complete burning to CO_2 and H_2O. At this point it is hard to propose any restricted number of surface modification agents for SnO_2 to achieve sensor response enhancement without additional information regarding the mechanism of conversion and the sensor response to the vapor of this compound.

3.6 Sensor Properties Studies

3.6.1 CO Sensing

The benchmark study of sensor sensitivity to CO, a common reducing gas, is of special interest since it allowed for the formation of general trends with respect to mechanisms of sensor sensitivity towards reducing gases [68].

The synthesized materials showed a different temperature dependence for sensor sensitivity to CO (40 ppm in air RH = 30 % Fig. 3.19). The material modified by catalytic clusters of Pd, had the largest sensor response at a low operating temperatures (200–250 °C). For most other materials, the sensor response, in contrast, increases with increasing operating temperature. Only in the case of SnO_2-Ru-700, this dependence passes through a maximum at 300 °C. At the high measurement temperature, 350 °C, the maximum sensor response was observed for the materials modified with catalytic clusters of gold. These differences indicate the various chemical mechanisms that underlie sensor sensitivity to CO.

The process of CO oxidation by different adsorbed oxygen species on the surface (O_2^-, O^- and O^{2-}) has a decisive contribution to the formation of an electrical signal in relation to CO in the case of materials based on nanocrystalline SnO_2 :

$$\beta \cdot CO_{(gas)} + O^{-\alpha}_{\beta(ads)} \rightarrow \beta \cdot CO_{2(gas)} + \alpha \cdot e^- \tag{3.33}$$

where $CO_{(gas)}$—the CO molecule in the gas phase, $O^{-\alpha}_{\beta(ads)}$—an atomic or molecular form of oxygen, e^-—an electron that is injected into the conduction band of the semiconductor, $CO_{2(gas)}$—the molecular reaction product desorbed from the surface.

In this context the low-temperature CO sensitivity of the Pd modified material is reasonable to connect to reaction (3.33) involving the above-discussed mobile forms of oxygen. Oxidation takes place according to the Eley-Riedel "collision" mechanism, which involves the oxidation of CO molecules in the gas phase, by atomic oxygen species, located on the PdO surface. This reaction occurs during rapprochement of two species, which in this case when a CO molecule passes near a solid surface with a partially oxidated Pd cluster [69]. We propose that the compensation of chemisorbed ionized forms of O^- expended on the oxidation of CO runs due to the phenomenon of reverse spillover—the transfer of already existing adsorbed O^- ions on the surface of SnO_2 to the clusters of Pd. This process leads to a change in the concentration of adsorbed oxygen on the surface of the semiconductor and, consequently, the change in electrical conductivity of the material that causes the sensor response to CO. With temperature increase, the process of re-oxidation of PdO_x accelerates due to the dissociation of molecular oxygen, adsorbed directly onto noble metal clusters. This phenomenon leads to a complete localization of the CO oxidation process on catalytic clusters and a

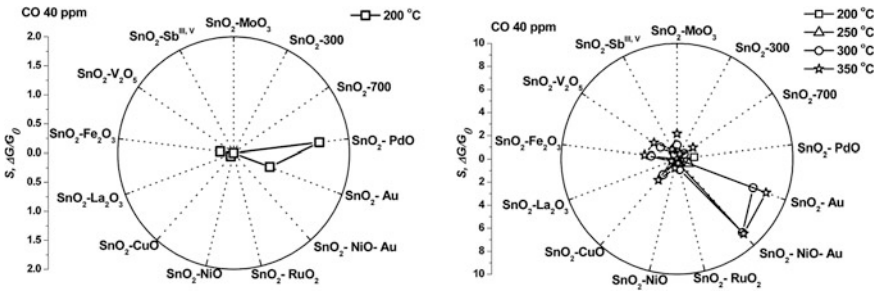

Fig. 3.19 Pattern of SnO_2-based materials sensitivity to CO (40 ppm in 30 %RH air) at low (200 °C) (*left*) and high (200–350 °C) working temperatures (*right*)

cessation of reverse spillover transport, which is accompanied by the disappearance of the sensor response to this gas.

A similar combination of factors underlies the sensor response to CO in the case of the material, modified by RuO_x clusters [70]. Displacement of the sensor response maxima in this case to the higher temperatures in comparison with the SnO_2-Pd-500 may be due to additional unusually high diffusion barriers in the case of the RuO_2 surface [71].

According to monotonous growth of the sensor response with increasing operating temperature in the case of other materials, the oxidation of adsorbed CO molecules occurs on the surface of the matrix SnO_2. The sharp rise in sensor response at a 300 °C working temperature in this context corresponds to the transition of molecular chemisorbed forms of O_2^- into the reactive atomic O^- discussed above. Thus we can assume that the participation of lattice oxygen in CO oxidation is secondary, because the growth of sensor response is observed at significantly lower operating temperatures of sensors than the temperature used to determine the activation barrier for Mars—van Krevelen type oxidation mechanism. The role of catalytic gold clusters in the case of materials showing the highest sensor response to CO, apparently, is activation of the oxygen species chemisorbed in the close vicinity to triple metal-oxide-gas interface [72, 73]. Despite the fact that this special form of oxygen is not dominant on the surface, it has extremely high reactivity. More accurate experimental data on this form of adsorbed oxygen on the surface of such materials to date are not available.

3.6.2 NH_3 Sensing

The main process that determines the sensor response of semiconductor metal oxide sensors to ammonia is usually postulated to be the oxidation of surface adsorbed NH_3 [74]:

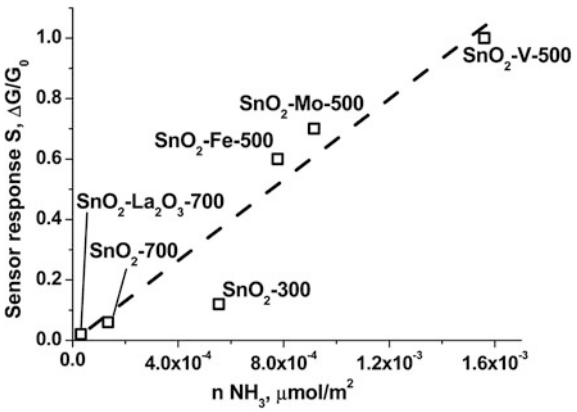

Fig. 3.20 Correlation between SnO_2-based materials surface brønsted acidity and sensor response towards NH_3 (20 ppm in humid air RH = 30 %, T = 200 °C)

$$2NH_{3(gas)} + \frac{3}{\beta} O^{-\alpha}_{\beta(ads)} \rightarrow N_{2(gas)} + 3H_2O + 3e^- \tag{3.34}$$

In accordance with the interconnection between surface acidity, molecular adsorption and sensor response the increase in the concentration of Brønsted acid sites on the surface in the case of materials modified with such acidic oxides as MoO_3 and V_2O_5 is accompanied by an increase in sensor response with respect to NH_3 gas (Fig. 3.20).

It must be noted, however, that this advantage in the magnitude of sensor signal is minuscule which respect to otherwise modified materials, which to some extent can be attributed to the competition of water vapor and NH_3 for surface adsorption on the same acidic sites. This phenomenon decreases ammonia adsorption thus limiting further steps for its oxidation on the surface, which leads to a reduction in the sensor response. At the same time in accordance to the data on the CO detection, materials, modified by gold, also express pronounced sensor response to ammonia since it exhibits a reducing nature as well as basic one (Fig. 3.21). The fall of the sensor response with increasing operating temperature, which is observed in the case of all tested materials, is likely due to a reduction in NH_3 adsorption [75]. It is important to note that the highest response towards NH_3 is for the case of SnO_2-Ru-700. The nature of this phenomenon could be explained with additional considerations on the chemical form of the modifier (Ru) on the sensor material surface. As it is introduced in the form of Ru(III) acetylacetonate with further annealing, an EPR study of this material (SnO_2-Ru-300) reveals a distinct signal, that corresponds to EPR-active Ru^{3+}. At the same time the interaction with reducing gas (NH_3) leads to an order of magnitude decrease of this signal indicating that Redox catalytic activity of this modifier is due to transition to oxidation states, other than Ru^{+3}. That might be Ru^0 and Ru^{+4} [76]. In this sense the presence of metallic form of Ru on the sensor material surface may activate the additional path of adsorbed ammonia conversion.

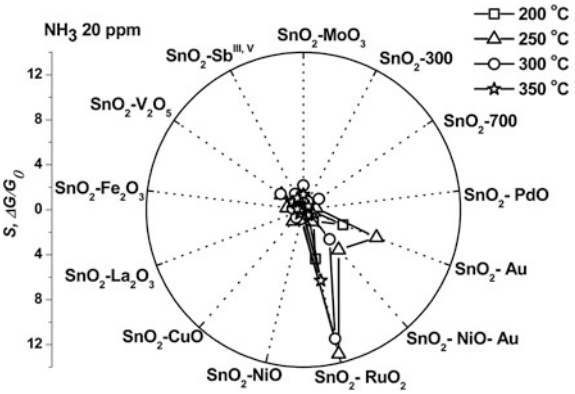

Fig. 3.21 Pattern of SnO_2-based materials sensitivity to NH_3 (20 ppm in humid air, RH = 30 %)

The metal surface of Ru is active in the catalytic dissociation of adsorbed molecular ammonia [77, 78] with formation of atomic nitrogen and hydrogen, desorbed in the molecular form:

$$NH_{3(gas)} + Ru(0001) \underset{k_{des}}{\overset{k_{ads}}{\longleftrightarrow}} NH_{3(ads)} + * \underset{k_{\det r}}{\overset{k_{diff}}{\longleftrightarrow}} NH_3 - * \xrightarrow{k_{diss}} N - * + 3H_{(ads)} \xrightarrow{k_{Ndiff}} N_{(ads)} + 3H_{(ads)} \tag{3.35}$$

with $NH_{3(gas)}$—a molecule of ammonia in the gas phase, Ru (0001)—Ru metal surface, $NH_{3(ads)}$—ammonia molecule adsorbed on a metal surface *—active site of dissociation of molecular ammonia, NH_3-*—ammonia molecule adsorbed at the center of the dissociation on the surface of metallic Ru, N−*—nitrogen atom adsorbed at the center of the dissociation on the surface of metallic Ru, $N_{(ads)}$—the nitrogen atom, which left the center of the dissociation, $H_{(ads)}$−adsorbed hydrogen atom.

Thus, despite the lack of experimental evidence it is reasonable to propose the formation of small amounts (clusters) of metallic ruthenium on the surface of Ru-modified SnO_2 during the interaction with reducing agents as a reason for especially pronounced response of this material towards ammonia. In addition, significant contributions to the chemical reactions on the surface are possible through the interaction of adsorbed species and atomic nitrogen via the formation of the nitrosyl species, NO, which is a chemical radical [79]:

$$N_{(ads)} + O^-_{(ads)} \rightarrow NO_{(ads)} + e^- \tag{3.36}$$

With its increased reactivity these newly formed nitrosyl species, NO, on the surface may play a role for additional centers of adsorption and chemical reaction of NH_3. These chemical processes may contribute significantly to the sensor response of SnO_2-Ru-700 with respect to ammonia, but this issue is generally unexplored as of yet.

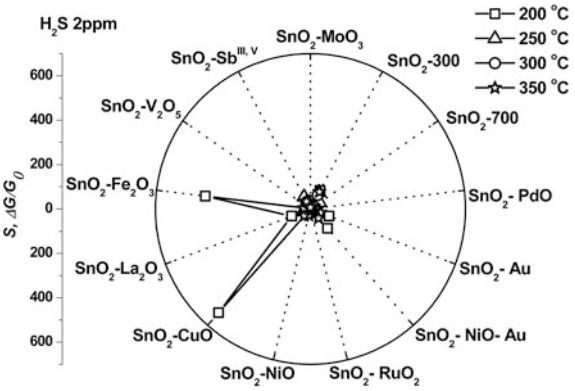

Fig. 3.22 Pattern of SnO_2-based sensor materials sensor response to H_2S (2 ppm in humid air, RH = 30 %)

3.6.3 H_2S Sensing

Materials modified with catalytic Au clusters, showing an increased sensor sensitivity to reducing gases, also have an elevated sensor response in the case of H_2S (Fig. 3.22), which is associated with the occurrence of the Redox process:

$$\beta \cdot H_2S_{(gas)} + 3O^{-\alpha}_{\beta(ads)} \rightarrow \beta \cdot SO_{2(gas)} + \beta \cdot H_2O_{(gas)} + 3\alpha \cdot e^- \tag{3.37}$$

The largest sensor response, however, was achieved for the case of the copper and iron oxide modified material, which in this case is likely caused by the chemical transformation of the material's surface.

In the case of nano SnO_2–CuO a significant change in resistance in the presence of H_2S should be attributed to the formation of copper (I) sulfide [80], which is a narrow-gap semiconductor:

$$6CuO + 4H_2S_{(gas)} = 3Cu_2S + SO_{2(gas)} + 4H_2O_{(gas)} \tag{3.38}$$

As a result of this reaction the energy barrier at the grain boundaries p-CuO/n-SnO_2 is removed and electrical conduction increases. A similar mechanism of sensor signal formation can be attributed to tin oxide modified with Fe_2O_3.

With an increase of the sensor working temperature, the sensor response of the material drops sharply, indicating that in these circumstances, a decisive contribution to the sensor response is made only by the process of oxidation of hydrogen sulfide to sulfur oxide by active species of oxygen adsorbed on the surface, preventing the formation of sulfides.

3.6.4 NO_2 Sensing

Despite the fact that the detailed mechanism of sensor response with respect to NO_2 is still a subject of debate, it was shown [63] that the change of the

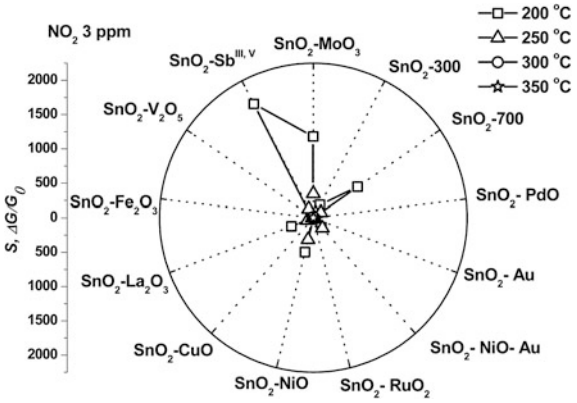

Fig. 3.23 Pattern of SnO_2-based sensor materials sensor response to NO_2 (3 ppm in humid air RH = 30 %)

conductivity of nanocrystalline SnO_2 in the presence of NO_2 molecules corresponds to the change in the concentration of adsorbed bidentate nitrite species:

$$NO_{2(gas)} + e^- \leftrightarrow NO^-_{2(ads)} \tag{3.39}$$

The increase in operating temperature sensor causes a decrease in sensor response due to desorption of NO_2 (Fig. 3.23).

In our study the increase of sensor signal in the case of several materials with the comparison to pure nanocrystalline tin dioxide was observed:

1. The most pronounced signal to nitrogen dioxide is obtained at 200 °C by means of SnO_2 doped with Sb. In this case the signal may be due to an electronic effect. Antimony introduction into tin dioxide is a well known route for increasing the density of electrons in the conduction band of semiconductor [81]. After the adsorption on the surface, the NO_2 molecule performs as an electronic trap, profoundly depleting the electron density in the conductance band and leading to significant decrease of nanocrystalline material conductance. So, the increase of concentration of electrons, which have enough energy to overcome the electric field resulting from the negative charging of the surface, favors reaction (3.39) that leads to the growth of sensor signal. The increase in working temperature greatly decreases the sensor response perhaps by a shift in the surface adsorption-desorption equilibrium of NO_2. This process also goes same way in the case of pure nanocrystalline SnO_2 that appears as the increase of sensor signal with SnO_2 crystallite size growth. Response growth with the transition from SnO_2-300 to the SnO_2-700, as described in the literature [82], has not yet found its comprehensive explanation, but it is proposed that this effect is caused by an increase in the charge carrier concentration in the conduction band of a semiconductor, which occurs with an increase in the crystallite size of SnO_2. This may be responsible for the shift of adsorption equilibrium (3.41). It cannot be excluded that the difference in charge carrier concentration in the presence of NO_2 molecules on the surface and in the pure air becomes greater for materials with large grain size and higher initial

concentration of free electrons in the surface layer in the atmosphere of pure air. It must be assumed that the same size effect is also responsible for increased sensitivity to NO_2, exhibited by the material SnO_2-La_2O_3-700;

2. in the case of SnO_2-MoO_3 the high sensitivity of this material with respect to NO_2 can be linked to the ability of Mo atoms to penetrate the surface layers of the SnO_2 grains and occupy lattice Sn positions in a variable oxidation state Mo^{+5} or Mo^{+6} [83–85]. Re-oxidation of Mo^{+5} to Mo $^{+6}$ upon NO_2 adsorption, probably leads to the formation of additional acceptor energy levels in the band gap, which are accompanied by a sharp drop in the material's surface conductivity. For materials modified with NiO a similar effect of "receptor" sensitivity may underlie their high sensitivity to NO_2.

3.6.5 Acetone Sensing

The similarity of the sensor sensitivity diagrams for sensor materials studied in relation to acetone (Fig. 3.24) and to CO indicates a possible similarity of mechanisms for the sensor response.

However, the low-temperature sensor response mechanism, observed in the case of CO for the materials modified by clusters of Pd, is not found during the detection of acetone. This may be related to the blocking of the reverse spillover mechanism caused by the decrease in concentration or mobility of chemisorbed oxygen on the surface of the oxide matrix. This restriction is lifted out at higher sensor operating temperature that allows SnO_2-Ru-700 material to show a maximum sensitivity to acetone vapor at 300 °C, similar to the process of detecting CO.

The maximum sensor signal with respect to acetone is exhibited by Au-modified materials, but only at a 350 °C working temperature. This indicates the complexity of the conversion process of acetone on the surface of materials flowing through a set of parallel mechanisms, rather than the simple oxidation to CO_2 and water.

The concentration dependence of the sensor response toward acetone (Fig. 3.25) has a linear form in double logarithmic coordinates at low concentrations.

The position of the tipping point of this linear dependence is proportional to the rate constants of interaction between the reducing gas and ionized adsorbed oxygen forms. In the simplest case it can be stated that the O^- oxygen formed on the surface of materials governs the conductivity of sensor layer [86]. The concentration of O^- adsorbed on the surface is governed by the interrelationship of oxygen dissociative adsorption on the surface of semiconductor oxide, O^- recombination and desorption and the process of interaction between O^- and adsorbed gas molecules.

$$O_{2(gas)} + 2e^- \underset{k_{-1}}{\overset{k_1}{\leftrightarrow}} 2O^-_{(ads)} \tag{3.40}$$

$$qO^-_{(ads)} + pA_{(ads)} \xrightarrow{k_2} products_{(ads)} + qe^- \tag{3.41}$$

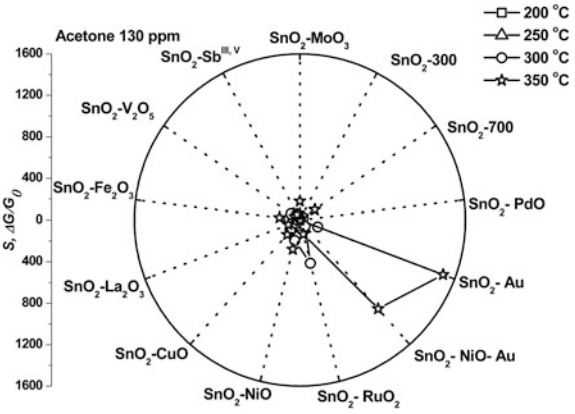

Fig. 3.24 Pattern of SnO_2-based materials sensor response to acetone (130 ppm in humid air, RH = 30 %)

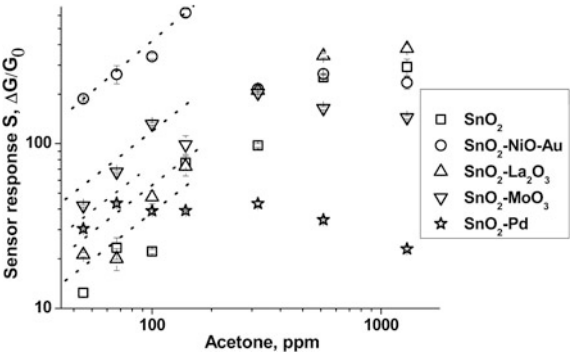

Fig. 3.25 *Calibration curves* of SnO_2-based sensor materials sensor response to acetone (T = 400 °C, dry air, RH = 4 %)

$$\frac{d\left[O_{ads}^{-}\right]}{dt} = k_1 P_{O_2}[e]^2 - k_{-1}\left[O_{ads}^{-}\right]^2 - k_2 P_A{}^p \left[O_{ads}^{-}\right]^q \tag{3.42}$$

where $O_{2(gas)}$ oxygen molecule in the gas phase, $O_{(ads)}^{-}$—ionized atomic form of adsorbed oxygen on the SnO_2 surface, $A_{(ads)}$- reducing gas molecule, adsorbed on the surface, P_{O2}- oxygen partial pressure in the gas phase, P_A- reducing gas partial pressure in the gas phase.

Since the sensor response is calculated at kinetic equilibrium state

$$\frac{d[O_{ads}^{-}]}{dt} = 0 \tag{3.43}$$

and the equation governing the $[O^-]$ concentration could be written as

$$\frac{k_1}{k_{-1}} P_{O_2}[e]^2 = [O^-]^2 \left(1 + \frac{k_2}{k_{-1}} P_A{}^p [O^-]^{q-2}\right) \tag{3.44}$$

For the detailed analysis of this equation and the interrelationships between sensor material conductance, sensor response and gases partial pressures the reader

is kindly asked to follow the [86] reference. For simplicity sake we must say that the sensor layer conductivity and sensor response is the interplay of semiconductor oxide physics and surface reactions chemistry. The relationship between the resistance of "ideal" SnO_2 with clean surface without any adsorbed oxygen or reducing gases (R_0) and actual resistance in air atmosphere with reducing gases present (R) is expressed as follows [86]:

$$\frac{R}{R_0} = \exp\left(\frac{m^2}{2}\right) \tag{3.45}$$

where

$$m = \frac{w}{L_D} \tag{3.46}$$

where w is the electron depletion layer thickness, L_D- Debye length—physical values, governing electric conductance of sensor layer. Further:

$$[e] = N_d \exp\left(-\frac{m}{2}\right) \tag{3.47}$$

$$[O^-] = N_d w \tag{3.48}$$

where N_d—concentration of donors, giving rise of electrons in conduction band of semiconductor oxide. In the case of SnO_2 them are oxygen vacancies in oxide lattice, serving as electron donors. The application of such notation gives one a possibility to introduce new form of Eq. 3.44:

$$\frac{\left(\frac{k_1}{k_{-1}} P_{O_2}\right)^{1/2}}{L_D} \cdot \exp\left(-\frac{m^2}{2}\right) = m\left(1 - \frac{k_2}{k_{-1}} P_A{}^p (N_d L_D m)^{q-2}\right)^{1/2} \tag{3.49}$$

Thus using new function, which is dependent only on reducing gas partial pressure at given reaction constants:

$$y = \frac{k_2}{k_{-1}} \left(N_d L_D\right)^{q-2}\Big)^{1/p} P_A \tag{3.50}$$

it is possible to numerically solve the relationship between R/R_0 (sensor response) and reducing gas concentration. The examples for different x (different k_1 to k_{-1} ratio) and different p and q (gas "reducing power") are shown on Fig. 3.26.

It must be noted that Yamazoe and Shimanoe [86] used R_0 as a resistance of semiconductor in a "flat band mode"—i.e. when nothing is adsorbed on the surface whereas we use R_0 for sensor response calculation as a resistance of semiconductor with surface covered with adsorbed oxygen to the highest extent possible in the measuring conditions. That's why the Fig. 3.25 looks like Fig. 3.26 rotated upside down.

According to this simplified model the increase of reducing gas partial pressure leads to a linear increase of sensor response (in double logarithmic coordinates)

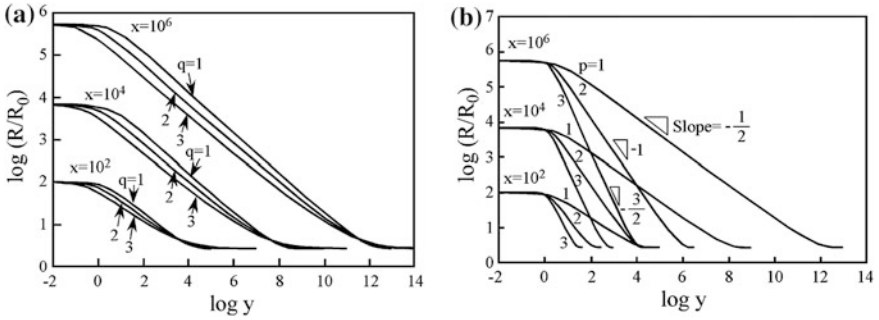

Fig. 3.26 Reduced resistance, R/R_0, as correlated with reduced reactivity of reducing gas, $y = \frac{k_2}{k_{-1}}(N_d L_D)^{\frac{q-2}{p}} P_A$ on logarithmic scales for complex surface reactions where q (a) and p (b) are varied. Variable $x = \frac{\frac{k_1}{k_{-1}} P_{O_2}}{L_D}$ reflects kinetic constant ratio given oxygen partial pressure is constant. ([86] With permission.)

only in restricted range of reducing gas partial pressure (i.e. reducing gas concentration). The k_2/k_{-1} ratio and p coefficient, given the oxygen partial pressure and k_1/k_{-1} ratio are fixed, governs the value of reducing gas concentration above which the further increase in concentration leads to no further increase in conductivity. Accordingly the sensor response also stops to rise. The height of linear slope above the X-axis (sensor response value) is governed by k_1/k_{-1} ratio—the higher the ratio, the bigger the response. The concentration regions of linear sensor response growth have the same slope in the case of all materials, with SnO_2-NiO-Au, demonstrating a significantly higher sensor response, which could be associated with a higher rate constant for dissociation of molecular O_2 on the surface of the material. In this sense the Au clusters role on the surface of SnO_2 in the increase of sensor response towards reducing gases is in the increase of k_1 constant—acceleration of molecular oxygen diffusion on the surface of oxide.

At the same time SnO_2-Pd-500 material manifests pronounced deviations in the form of calibration curve and the length of the concentration range with linear growth of sensor response. This notion is in line with considerations of differences in sensor response mechanisms for this material and other tested samples, based on oxidation processes carried on top of the Pd clusters coupled with adsorbed O^- transfer via reverse spillover mechanism.

In line with these arguments gas chromatographic analysis has shown a connection between a sharp rise in the sensor response with the degree of conversion of acetone (Fig. 3.27) as the working temperature rises. The analysis was made through the use of a special setup which allows the detection of products formed via acetone interaction with the sensor materials under the same conditions as the sensor experiments are made. This type of experiment can be generally characterized as an ‘operando’ experiment as discussed in the Gurlo chapter.

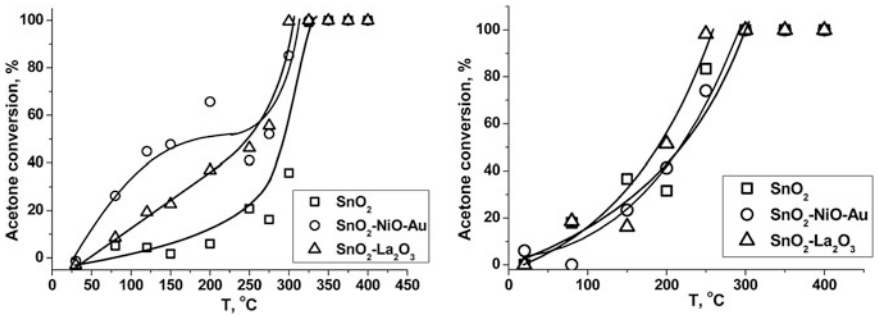

Fig. 3.27 Acetone conversion with temperature rise—1,800 (*left*) and 200 (*right*) ppm in dry air

Analysis of the chromatographic peaks (Fig. 3.28) suggests the formation of a large number of products of incomplete conversion of acetone at low operating temperatures and a decisive contribution of their complete oxidation to CO_2 and H_2O towards the sensor response magnitude. This in total can be described by the equation:

$$(CH_3)_2CO_{gas} + \frac{8}{\beta}O^{-\alpha}_{\beta(ads)} \rightarrow 3CO_{2gas} + 3H_2O_{(gas)} + \frac{8\alpha}{\beta}e^- \tag{3.51}$$

At the same time GC/MS analysis showed a number of complex compounds, formed during interaction even at maximum operating temperatures that have bigger molar masses than that of acetone.

Two of such condensation products has been identified as 2,4-dimethylfuran and 3-pentene-2-on :

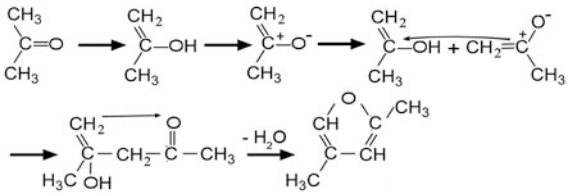

(3.52)

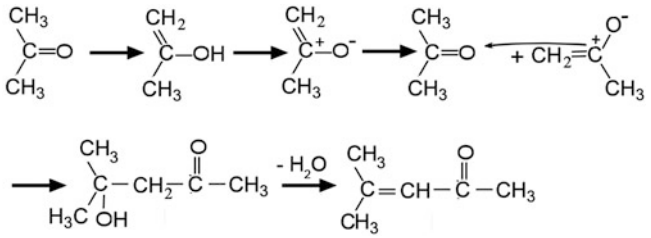

(3.53)

The accumulation of such substances on the sensor material's surface leads to the blocking of the molecular O_2 adsorption and dissociation centers, which is

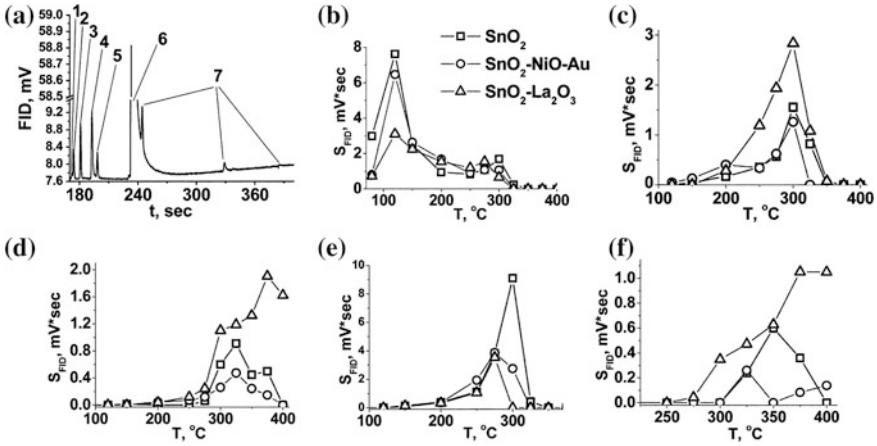

Fig. 3.28 **a** Chromatogram of products mixture obtained after acetone (1,800 ppm) interaction with sensor material (SnO_2-500) at T = 300 °C. **b–f** Comparative graphs of absolute content in products mixture exhausted from reactor vs. temperature of acetone (1800 ppm) interaction with sensor material (SnO_2-500)

Table 3.4 Selection of modifiers for SnO_2-based gas sensors with enhanced selectivity

Target gas	Interaction with the surface of n-type semiconductor oxide, resulting in conductance change	Suitable modifier
Reducing gases		
without pronounced acid/base properties: CO, H_2, CH_4	Oxidation by chemisorbed oxygen	Noble metals and their oxides, Au
Lewis bases: NH_3, amines	Oxidation by chemisorbed oxygen; Adsorption on surface acid sites	Metal oxides more acidic than SnO_2: V_2O_5, MoO_3, WO_3
Acids: H_2S	Oxidation by chemisorbed oxygen; Heterolytic reaction with Lewis acid/base pair on oxide surface	Metal oxides more basic than SnO_2: Fe_2O_3, In_2O_3, La_2O_3
Complex organic molecules with different functional groups:	Oxidation by chemisorbed oxygen;	Noble metals and their oxides, Au
Oxidizing gases		
O_2, NO_2, O_3	Chemisorption with localization of electrons from oxide conduction band	Noble metals and their oxides, Au; Electron donor additives: Sb(V); Modifiers, which can increase their oxidation state during interaction with oxidizing gas Mo(V), Ni(II)

accompanied by decrease in the conversion of acetone via the total oxidation reaction (3.40), leading to a decrease in sensor response.

Comparative analysis has shown that introduction of catalytic clusters of Au on the SnO_2 surface, leads to an increase in acetone conversion, a reduction in the formation of heavy products of the acetone conversion on the surface of the SnO_2-based sensor materials and an increase in the value of the sensor signal perhaps due to enhanced acetone combustion to CO_2 and H_2O.

3.7 Concluding Remarks

On the basis of the sensor response patterns towards CO, acetone, NH_3, H_2S and NO_2 one can conclude that chemical modification of SnO_2 with different catalysts provides an effective route for tailoring sensor materials with enhanced selectivity towards the detection various gas molecules. To predict the most suitable modifier to maximize the SnO_2 sensor response to any particular gas it is necessary to analyze the chemical nature of the interaction between semiconductor matrix, modification agent and the target gas molecule. These conclusions are summarized in Table 3.4:

However, it is currently impossible to establish a parameter, which would clearly link the fundamental properties of modifiers with their catalytic activity and their influence on SnO_2 sensor properties. The final optimization of the sensor material should be based on the requirements determined by practical tasks: sensitivity, response and recovery time, energy consumption, working temperature, precision of measurements, long term stability. In each case it is necessary to take into account the following factors:

- Tin oxide nanostructure;
- Concentration of modifier and its distribution between surface and bulk of tin oxide crystallites;
- Humidity;
- Target gas concentration range;
- Possible poisoning of sensor material.

Accounting for these factors still require detailed experimental studies to resolve specific practical problems.

References

1. Takahata K (1988) Tin oxide sensors—development and applications, highly sensitive SnO_2 gas sensors for volatile sulfides. In: Seiyama T (ed) Chemical sensor technology. Elsevier, Amsterdam, pp 39–55
2. Souteyrand E (1997) Transduction electrique pour la detection de gaz. Les capteurs chimiques, CMC2, Lyon, pp 15–35

3. Gouma PI (2003) Nanostructured polymorphic oxides for advanced chemosensors. Rev Adv Mater Sci 5:147–154
4. Norris JOW (1987) The role of precious metal catalysts in solid state gas sensorsgas sensors. In: Mosely PT, Tofield BC (eds) Alam higher. Bristol and Philadelphia, pp 124–138
5. Idriss H, Barteau MA (2000) Active sites on oxides: from single crystalsingle crystals to catalysts. Adv Catal 45:261–331
6. Vol'kenstein FF (1963) The electronic theory of catalysis on semiconductors. Pergamon, Oxford
7. Calatayud M, Markovits A, Menetrey M, Mguig B, Minot C (2003) Adsorption on perfect and reduced surfaces of metal oxides. Catal Today 85:125–143
8. Busca G (1999) The surface acidity of solid oxides and its characterization by IR spectroscopic methods. An attempt at systematization. Phys Chem 1:723–736
9. Barthomeuf D (1984) Conjugate acid-base pairs in zeolites. J Phys Chem 88:42–45
10. Niwa M, Habuta Y, Okumura K, Katada N (2003) Solid acidity of metal oxide monolayer and its role in catalytic reactions. Catal Today 87:213–218
11. Auroux A, Gervasini A (1990) Microcalorimetric study of the acidity and basicity of metal oxide surfaces. J Phys Chem 94:6371–6379
12. Duffy A, Ingram MD (1971) Establishment of an optical scale for Lewis basicity in inorganic oxyacids, molten salts, and glasses. J Am Chem Soc 93:6448–6454
13. Duffy A (1993) A review of optical basicity and its applications to oxidic systems. Geochim Cosmochim Acta 57:3961–3970
14. Duffy JA (1986) Chemical bonding in the oxides of elements: a new appraisal. J Solid State Chem 62:145–157
15. Tessman JR, Kahn AH, Shockley W (1953) Electronic polarizabilities of ions in crystals. Phys Rev 92:890–895
16. Zhang Y (1982) Electronegativities of elements in valence states and their applications. 1 Electronegativities of elements in valence states. Inorg Chem 21:3886–3889
17. Zhang Y (1982) Electronegativities of elements in valence states and their applications. 2 A scale fro strength of Lewis acids. Inorg Chem 21:3889–3893
18. Portier J, Campet G, Etourneau J, Tanguy B (1994) A simple model for the estimation of electronegativities of cations in different electronic states and coordinations. J Alloys Compd 209:285–289
19. Portier J, Campet G, Etorneau J, Shastry MCR, Tanguy B (1994) A simple approach to materials design: role played by an ionic-covalent parameter based on polarizing power and electronegativity. J Alloys Compd 209:59–64
20. Moriceau P, Lebouteller A, Bodres E, Courtine P (1999) A new concept related to selectivity in mild oxidation catalysis of hydrocarbons: the optical basicity of catalyst oxygen. Phys Chem 1:5735–5744
21. Sanderson RT (1951) An interpretation of bond lengths and a classification of bonds. Science 114:670–672
22. Sanderson RT (1975) The interrelationship of bond dissociation energies and contributing bond energies. J Am Chem Soc 97:1367–1372
23. Jeong NCh, Lee JS, Tae EL, Lee YoJ, Yoon KB (2008) Acidity scale for metal oxides metal oxides and sanderson's electronegativities of Lanthanide Elements. Angew Chem Int Ed 120:10282–10286
24. Henry M (1994) Partial charges distributions in crystalline materials through electronegativity equalization. Mater Sci Forum (152–153), pp 355–358
25. Nortier P, Borosy AP, Allavena M (1997) ab initio Hartree-Fock study of bronsted acidity at the surface of oxides. J Phys Chem B 101:1347–1354
26. Berholic J, Horsley JA, Murrel LL, Sherman LG, Soled S (1987) Bronsted acid sites in transition metal transition metal oxide catalysts: modeling of structure, acid strengths and support effects. J Phys Chem 91:1526–1530
27. Shiga A, Katada N, Niva M (2006) A theoretical study on bronsted acidity of WO_3 clusters supported on metal oxide supports by "paired interacting orbitals" (PIO) analysis. Catal Today 111:333–337

28. Mars P, van Krevelen DW (1954) Oxidations carried out by means of vanadium oxide catalysts. Chem Eng Sci (Spec Suppl) 3:41–59
29. Ali AM, Emanuelsson EAC, Patterson DA (2010) Photocatalysis with nanostructured zinc oxide thin films: the relationship between morphology and photocatalytic activity under oxygen limited and oxygen rich conditions and evidence for a Mars—Van Krevelen mechanism. Appl Catal B(97):168–181
30. Finocchio E, Busca G, Lorenzelli V,Willey RJ (1994) FTIR Studies on the selective oxidation and combustion of light hydrocarbons at metal oxide surfaces. J Chem Soc Faraday Trans 90:3347–3356
31. Over H, Kim YD, Seitsonen AP, Wendt S, Lundgren E, Schmid M, Varga P, Morgante A, Ertl G (2000) Atomic-scale structure and catalytic reactivity of the RuO_2(110) surface. Science 287:1474–1476
32. Han W-P, AI M (1982) The φ-classification of metal oxides for heterogeneous oxidation catalysts. J Catal 78:281–288
33. Bielański A, Haber J (1979) Oxygen in catalysis on transition metal oxides. Cat Rev—Sci Eng 19:1–41
34. Catlow CRA, Jackson RA, Thoma JM (1990) Computational studies of solid oxidation catalystst. J Phys Chem 94:7889–7893
35. Reddy BM (2006) Redox properties of metal oxides. In: Fierro JLG (ed) Metal oxides: chemistry and applications. CRC Press, Taylor & Francis Group, Boca Raton, pp 215–246
36. Busca G, Finocchio E, Ramis G, Ricchiardi G (1996) On the role of acidity in catalytic oxidation. Catal Today 32:133–143
37. Panov GI, Dubkov KA, Starokon EV (2006) Active oxygen in selective oxidation catalysis. Catal Today 117:148–155
38. Liu H-F, Liu R-S, Liew KY, Johnson RE, Lunsford JH (1984) Partial oxidation of methane by nitrous oxide over molybdenum on silica. J Am Chem Soc 106:4117–4121
39. Schlogl R (2001) Theory in heterogenous catalysis. Cattech 5:146–170
40. Grzybowska-Swierkosz B (2002) Effect of additives on the physicochemical and catalytic properties of oxide catalysts in selective oxidation reactions. Top Catal 21:35–46
41. Rumyantseva MN, Gaskov AM (2008) Chemical modification of nanocrystalline metal oxides: effect of the real structure and surface chemistry on the sensor properties. Russ Chem Bull 57:1106–1125
42. Yushchenko VV (1997) Calculation of the acidity spectra of catalysts from temperature-programmed ammonia desorption data. Russian J Phys Chem 71:547–550
43. Burmistrov VA (1986) Hydrated oxides of IV and V groups (in Russian). Nauka, Moscow, p 160
44. Abee MW, Cox DF (2002) NH_3 chemisorption on stoichiometric and oxygen-deficient SnO_2 (110) surfaces. Surf Sci 520:65–77
45. York SC, Abee MW, Cox DF (1999) α-Cr2O3 (#): surface characterizationcharacterization and oxygen adsorption. Surf Sci 437:386–396
46. Abee MW, Cox DF (2001) BF3 adsorptionadsorption on r-Cr2O3 (#): probing the lewis basicity of surface oxygen anions. J Phys Chem B 105:8375–8380
47. Maier J, Göpel W (1988) Investigations of the bulk defect chemistry of polycrystalline Tin(IV) oxide. Thin Solid Films 72:293–302
48. De Wit JHW, Van Unen G, Lahey M (1977) Electron concentration and mobility in In_2O_3. J Phys Chem Solids 38:819–824
49. Barŝan N, Weimar U (2001) Conduction model of metal oxide gas sensors. J Electroceram 7:143–167
50. Morrison SR (1977) The chemical physics of surfaces. Plenum, New York
51. Rumyantseva MN, Makeeva EA, Badalyan SM, Zhukova AA, Gaskov AM (2009) Nanocrystalline SnO_2 and In_2O_3 as materials for gas sensors: the relationship between microstructure and oxygen chemisorption. Thin Solid Films 518:1283–1288
52. Descorme C, Duprez D (2000) Oxygen surface mobility and isotopic exchange on oxides: role of the nature and the structure of metal particles. Appl Catal A 202:231–241

53. Martin D, Duprez D (1996) Mobility of surface species on oxides. 1 Isotopic exchange of $^{18}O_2$ with ^{16}O of SiO_2, Al_2O_3, ZrO_2, MgO, CeO_2, and CeO_2-Al_2O_3. Activation by noble metals. Correlation with oxide basicity. J Phys Chem 100:9429–9438
54. Haruta M (2004) Nanoparticulate goldgold catalysts for low-temperature CO oxidation. J New Mat Electrochem Systems 7:163–172
55. Montmeat P, Marchand J-C, Lalauze R, Viricelle J-P, Tournier G, Pijolat C (2003) Physico-chemical contribution of goldgold metallic particles to the action of oxygen on tin dioxide sensors. Sens Act B 95:83–89
56. Conner WC, Falconer JL (1995) Spillover in heterogeneous catalysis. Chem Rev 95:759–788
57. Aksel S, Eder D (2010) Catalytic effect of metal oxides on the oxidation resistance in carbon nanotube-inoragnic hybrids. J Mater Chem 20:9149–9154
58. http://webbook.nist.gov
59. Davydov AA (2003) Molecular spectroscopy of oxide catalyst surfaces. Wiley, Chichester, p 641
60. Zhou Z, Gao H, Liu R, Du B (2001) Study of structure and property for the electron transfer system. Theochem 545:179–186
61. Šulka M, Pitoňák M, Neogrády P, Urban M (2008) Electron affinity of the O2 molecule: CCSD(T) calculations using the optimized virtual orbitals space approach. Int J Quantum Chem 108:2159–2171
62. Sergent N, Epifani M, Comini E, Faglia G, Pagnier T (2007) Interactions of nanocrystalline tin oxide powder with NO_2: a Raman spectroscopic study. Sens Act B 126:1–5
63. Prades JD, Cirera A, Morante JR, Pruned JM, Ordejón P (2007) Ab initio study of NOx compounds adsorption on SnO_2 surface. Sens Act B 126:62–67
64. Leblanc E, Perier-Camby L, Thomas G, Giber G, Primet RM, Gelin P (2000) NOx adsorption onto dehydroxylated or hydroxylated tin oxide surface. Application to SnO2-based gas sensorsgas sensors. Sens Act B 62:67–72
65. Golodets GI, Borovik VV, Vorotyntsev VM (1986) Mechanism and kinetics of selective catalytic oxidation of acetone. Theor Exper Chem 22:235–237
66. Harrison PG, Thornton EW (1976) Tin oxide surfaces. Part 7—an infrared study of the chemisorption and oxidation of organic Lewis base molecules on tin (IV) oxide. J Chem Soc Faraday Trans I(72):2484–2491
67. Pierce KG, Barteau MA (1995) Ketone coupling on reduced TiO_2 (001) surfaces: evidence of pinacol formation. J Org Chem 60:2405–2410
68. Barŝan N, Koziej D, Weimar U (2007) Metal oxide-based gas sensor research: How to? Sens Act B 121:18–35
69. Hirvi JT, Kinnunen T-JJ, Suvanto M, Pakkanen TA, Nørskov JK (2010) CO oxidation on PdO surfaces. J Chem Phys 133:084704
70. Šljivančanin Ž, Hammer B (2010) CO oxidation on fully oxygen covered Ru (0001): role of step edges. Phys Rev B 81:121413 R
71. Seitsonen AP, Over H (2009) Intimate interplay of theory and experiments in model catalysiscatalysis. Surf Sci 603:1717–1723
72. Wang S, Wang Y, Jiang J, Liu R, Li M, Wang Y, Su Y, Zhu B, Zhang S, Huang W, Wu S (2009) A DRIFTS study of low-temperature CO oxidation over AuAu/SnO_2 catalyst prepared by co-precipitation method. Catal Commun 10:640–644
73. Hakkinen H, Abbet S, Sanchez A, Heiz U, Landman U (2003) Structural, electronic and impurity-doping effects in nanoscale chemistry: supported goldgold nanoclusters. Angew Chem Int Ed 42:1297–1300
74. Rout CS, Hegde M, Rao CNR (2007) Ammonia sensors based on metal oxide nanostructures. Nanotechnology 18:205504
75. Mortensen H, Diekhoner L, Baurichter A, Jensen E, Luntz AC (2000) Dynamics of ammonia decomposition on Ru (0001). J Chem Phys 113:6882–6887
76. Marikutsa AV, Rumyantseva MN, Gaskov AM, Konstantinova EA, Grishina DA, Deygen DM (2011) CO and NH_3 sensor properties and paramagnetic centers of nanocrystalline SnO_2 modified by Pd and Ru. Thin Solid Films. Accepted for publication

77. Ganley JC, Thomas FS, Seebauer EG, Masel RI (2004) A priori catalytic activity correlations: the difficult case of hydrogen production from ammonia. Catal Lett 96:117–122
78. Hansgen DA, Vlachos G, Chen JG (2010) Using first principles to predict bimetallic catalysts fort he ammonia decomposition reaction. Nat Chem 2:484–489
79. Boccuzzi F, Guglielminotti E (1994) IR study of TiO_2-based gas-sensor materials: effect of ruthenium on the oxidation of NH3, $(CH_3)_3N$ and NO. Sens Act B 21:27–31
80. Pagnier T, Boulova M, Galerie A, Gaskov A, Lucazeau G (2000) Reactivity of SnO_2–CuO nanocrystalline materials with H_2S: a coupled electrical and Raman spectroscopic study. Sens Act B 71:134–139
81. Jeon H, Jeon M, Kang M, Lee S, Lee Y, Hong Y, Choi B (2005) Synthesis and characterization of antimony doped tin oxide (ATO) with nanometer-sized particles and their conductivities. Mater Lett 59:1801–1810
82. Rumyantseva MN, Gaskov AM, Rosman N, Pagnier T, Morante JR (2005) Raman surface vibration modes in nanocrystalline SnO_2 prepared by wet chemical methods: correlations with the gas sensors performances. Chem Mater 17:893–901
83. Kaur J, Vankar VD, Bhatnagar MC (2008) Effect of MoO_3 addition on the NO_2 sensing properties of SnO_2 thin films. Sens Act B 133:650–655
84. Ivanovskaya M, Lutynskaya E, Bogdanov P (1998) The influence of molybdenum on the properties of SnO_2 ceramic Sensors. Sens Act B 48:387–391
85. Chiorino A, Ghiotti G, Prinetto F, Carotta MC, Gallana M, Martinelli G (1999) Characterization of materials for gas sensors: surface chemistry of SnO_2 and MoO_x–SnO_2 nano-sized powders and electrical responses of the related thick films. Sens Act B 59:203–209
86. Yamazoe N, Shimanoe K (2008) Theory of power laws for semiconductor gas sensors. Sens Act B 128:566–573
87. Gellings PJ, Bouwmeester HJM (2000) Solid state aspects of oxidation catalysis. Catal Today 58:1–53